Marine Geology
May 2024, Volume 471, Pages 107281 (20p.)
https://doi.org/10.1016/j.margeo.2024.107281
https://archimer.ifremer.fr/doc/00885/99725/

Suspended particulate matter dynamics at the interface between an estuary and its adjacent coastal sea: Unravelling the impact of tides, waves and river discharge from 2015 to 2022 in situ high-frequency observations

Verney Romaric [1, *], Le Berre David [1], Repecaud Michel [2], Bocher Alan [3], Bescond Tanguy [3], Poppeschi Coline [4], Grasso Florent [1]

[1] Ifremer, DYNECO-DHYSED, CS10070, 29280 Plouzane, France
[2] Ifremer, RDT-LBCM, CS10070, 29280 Plouzane, France
[3] Ifremer, RDT-SIIM, CS10070, 29280 Plouzane, France
[4] Ifremer, Univ. Brest, CNRS, IRD, Laboratory for Ocean Physics and Satellite remote sensing (LOPS), IUEM, 29280 Brest, France

* Corresponding author : Romaric Verney, email address : romaric.verney@ifremer.fr

Abstract :

Suspended particulate matter (SPM) dynamics and exchange fluxes at the interface between a macrotidal estuary and its adjacent coastal sea were investigated from long-term high-frequency in situ observations. Optical and acoustic measurements were coupled to calculate SPM concentration over the whole water column using an existing acoustic inversion algorithm. A method was developed to distribute over the water column the surface and bottom calibrated equivalent particle diameters based on complementary ship-based surveys. Surface and bottom SPM show similar patterns in response to main forcings (tide, river discharge and waves), but present significantly higher concentrations near the bed. Increasing tidal ranges were responsible for higher tidal-median SPM concentrations, with spring/neap SPMC ratio varying from 2 to 3. This increase is driven by local resuspension during flood phase at the bottom, and low salinity turbid water flushed out from the estuary from mid-ebb to low tide at the surface. Increasing river discharge implies a downward shift of the estuarine turbidity maximum from the inner estuary to the mouth, and yields a 2-fold increase in both surface and bottom tidal-median concentration. Waves generated strong resuspension, with the highest SPM concentration recorded both at the surface and near the bed. Analysing SPM residual fluxes highlighted large up-estuary fluxes from low to moderate tidal ranges (below 6 m), and exporting seaward fluxes for higher tidal ranges, due to stronger mixing during spring tides. High river discharge enhanced stratification at the mouth and strengthened density circulation and up-estuary residual bottom circulation, resulting in larger up-estuary fluxes for all tidal ranges. Larger SPM concentrations along the tidal cycle during wave events yield high exporting fluxes.

Highlights

► Long term high frequency observations were analyzed to investigate the sediment dynamics at the interface between estuary and coastal sea ► An original approach was developed to unify and inverse acoustic backscatter signal to SPM concentration ► Instantaneous and residual sediment fluxes were computed and analyzed to apprehend sediment exchange dynamics between the estuary and the coastal sea in response to riverine and oceanic forcings.

Keywords : Estuary-coastal sea interface, Sediment dynamics, Long term monitoring, Acoustic backscatter inversion, Fluxes

2. Introduction

Estuary-coastal systems (ECS) represent a critical area in the land-sea continuum, providing essential functions and services for both the ecosystem and the society, and is threatened by human activities and climate change (Costanza et al., 1997; Lotze et al., 2006; Worm et al., 2006). ECS are featured by strong morphological, hydrological and biogeochemical gradients, structuring a mosaic of habitats and hence sheltering rich biodiversity. For several decades, ECS faced multiple challenges, potentially conflicting with a sustainable management (Halpern et al., 2008; Worm et al., 2006): preserving their predominant ecological value together with providing essential ecosystem services (e.g. fisheries, maritime traffic); improving water quality (Rodrigues et al., 2020) together with adapting to climate change effects (Dunn et al., 2019; Nicholls and Cazenave, 2010).

Investigating suspended particulate matter (SPM) dynamics and fluxes in the ECS can contribute to understanding and anticipating future trajectories of these systems. Indeed, SPM are transported all along the land-sea continuum. Understanding the mechanisms controlling these fluxes is essential to address multiple challenges: i) nutrients and pollutants of various origin are adsorbed on SPM, hence water quality issue is closely related to SPM dynamics; ii) SPM through turbidity and light penetration depth contributes to control primary production (Cloern, 1987; Wetsteyn and Kromkamp, 1994); iii) while transported downward, SPM accumulate in estuarine turbidity maximum (ETM)

areas (Burchard et al., 2018), creating a typical environment where organic and mineral SPM can interact and be intensively transformed (Manning et al., 2006; Morelle et al., 2018), with direct consequences on water quality (Etcheber et al., 2011). Moreover, SPM fluxes and predominantly their mineral content drive the morphological evolution and sediment budget of ECS: migration of subtidal banks, evolution of lateral intertidal flats, siltation in the main channel(s) (Cox et al., 2021; Schulz et al., 2018; Wang et al., 2018). The latter yield to nearly continuously extensive maintenance dredging works to keep navigable channels (Cox et al., 2021; Lemoine and Le Hir, 2021). Finally, modifications in SPM fluxes due to climate change effects are crucial for the fate of estuarine habitats, and the functions they support (Leuven et al., 2019).

Within ECS, the estuarine dynamics and its consequences on ETMs have been largely explored, from *in situ* measurements (Jalón-Rojas et al., 2016, 2015; Jay et al., 2015; McSweeney et al., 2016; Moskalski et al., 2020; Sommerfield and Wong, 2011; Sottolichio et al., 2011) and modelling studies (Burchard and Baumert, 1998; Gong et al., 2022; Grasso et al., 2018; Hesse et al., 2019; Liu et al., 2023), leading to consolidated review papers (Burchard et al., 2018; Geyer and MacCready, 2014). These studies highlighted the importance of tides and river discharge on key sediment transport mechanisms: tidal pumping and density circulation induced by longitudinal and vertical stratification inside estuaries. Moving seaward, the interface between estuary and coastal sea is much less observed while not less complex, due to the strong competition between tides, river discharge and waves, generating large vertical gradients due to low-salinity-turbid surface plumes or intense bottom resuspension by tidal currents and waves (Chapalain et al., 2019). Together with modelling studies (e.g. Diaz et al., 2020; Grasso et al., 2021; Schulz et al., 2018), most existing observations are mainly ship-based surveys or short-term deployments (from weeks to months), that focus on limited typical events (Chapalain et al., 2019; Figueroa et al., 2020; Liu et al., 2011; Schettini et al., 2013; Uncles et al., 1985). However, understanding sediment transport regimes at the mouth of estuaries and how waves, tides and river discharge interact and drive SPM dynamics and sediment exchange between estuaries and coastal seas is essential to anticipate the morphological evolutions of ECS, and at the ecosystem scale their capacity to maintain their functions and services.

In the present study, we aim to unravel the relative contribution of tides, river discharge and waves on SPM dynamics and SPM fluxes at the interface between the estuary and the coastal sea using in situ data. We investigate physical mechanisms through observations in regions that are typically only explored with numerical models (Diaz et al., 2020; Grasso et al., 2021; Schulz et al., 2018). This work is supported by a long-term observation time series (2015-2022) at the SCENES coastal observation station, providing multi-source observations (CTD, optical and acoustic sensors) for a wide range of hydro-meteorological conditions. This dataset is concurrently used to analyse the influence of extreme forcing events on the SPM dynamics at the interface between estuary and coastal sea (see Poppeschi et al., submitted).

3. Methods

3.1. Study site

The Seine Estuary-sea continuum connects a 170km-long macrotidal estuary (with semi-diurnal tides, tidal range (TR)>7m during highest spring tides, TR<3m during lowest neap tides) and a large bay (100x50km^2, 30m depth on average, and shallower than 45m). The main tributary is the Seine River, characterized by a mean discharge (Q) of ~410m^3/s and flood events exceeding 800m^3/s and reaching up to 2000m^3/s, mainly during winter and early spring. During summer, Q reaches the lowest values, below 200m^3/s and down to 100m^3/s during the driest years.

The Bay of Seine is partly protected from Atlantic Ocean swells but storm winds blowing from west to north-east generate intense local wave events generally from October to April. At the mouth of the estuary (depth ~15m), waves can reach 3 to 4m and periods from ~8s to 10s.

This system is highly engineered, with the presence of Le Havre and Rouen harbours, submersible dikes channelizing the tidal flow at the mouth, and intense, continuous dredging to maintain or

enhance navigability (Figure 1) (Avoine et al., 1981; Grasso and Le Hir, 2019; Lemoine and Le Hir, 2021).

The Seine system is a mixed-sediment environment, with both mud and sand. At the mouth, sand banks are present on each side of the main channel, and mud covers large lateral intertidal areas. Subtidal areas feature a mosaic of mud-sand facies (Lesourd et al., 2016) with sand offshore and muddy fine sand-mud facies in the mouth. The Seine Estuary has a strong estuarine turbidity maximum, and its dynamics is very well documented with both in situ (Avoine, 1981; Sahin et al., 2017; Druine et al., 2018, Grasso et al., 2018) and numerical model studies (Brenon and Le Hir, 1999; Le Hir et al., 2001; Chauchat et al., 2009; Grasso et al., 2018). This ETM is characterized by strong near-bottom SPM concentration ((SPMC)~1 to 4 g/l; Avoine, 1981; Grasso et al., 2018), located, on average, 20km upstream of the estuary mouth (i.e. ~kilometric point (kp) 350 - kilometric distance from Paris). Depending on tidal ranges and river discharge, the tidally-averaged ETM position can move from the mouth (kp 365 – Q>1500m^3/s) to 20 to 30km upstream of the estuary (i.e. kp 340) for Q<200m^3/s (Grasso et al., 2018). The influence of the ETM and waves as well as human activities also drives the morphological evolution of the mouth, and especially mudflat dynamics, as observed by Deloffre et al. (2006), Cuvilliez et al. (2009) and Verney et al. (2007) or simulated by Le Hir et al. (2001), Waeles et al. (2007) and Mengual et al. (2021). However, less is known about the SPM dynamics at the interface between the estuary mouth and the bay. Most studies are based on numerical models, evaluating hydrodynamics and SPM dynamics and fluxes for different forcing or morphological conditions (Schulz et al., 2018; Grasso et al., 2021). In situ observations at this interface are rare, and mainly correspond to short-term and episodic measurements (Avoine, 1981; Chapalain et al., 2018), thus not providing a robust pluri-annual evaluation of the SPM dynamics and fluxes in response to dynamic forcings.

The SCENES observatory is located in the north-western part of the Seine mouth, at the interface between the estuary and bay (49°28.844 N; 0°01.908 E), with a 15.8 m depth (mean sea level – percentile 1: 12m – percentile 99: 19m). From field surveys in 2016, Chapalain et al. (2019) observed

neap and spring tidal dynamics at this location, showing intense flood currents during spring, exceeding 1m/s, and lower ebb currents (~0.5m/s). They also observed a strong subsurface stratification at low tide (from 20 to 30PSU at surface compared with marine salinity ranging from 31PSU to 33PSU) when the estuarine freshwater is flushed out from the estuary to the bay. These estuarine waters are associated with SPMC reaching 50mg/l during spring tide and 10mg/l during neap tide. Near bottom (2m above the bed), Chapalain et al. (2019) also observed strong resuspension mainly during flood, with SPMC values reaching 150mg/l during spring tide, but staying below 30mg/l during neap tides.

3.2. *Hydro-meteorological and tidal forcing parameters*

The tidal gauge at Le Havre (mouth of the Seine Estuary) provides the tidal range time series (http://datashom.fr). The river discharge is measured daily at the Vernon gauging station, located upstream the estuary tidal limit (www.hydro.eaufrance.fr), 200km up the mouth. According to Artelia (2019), we consider that the propagation time of the river flow to the mouth is on average 5 days.

To work with a continuous wave dataset, wave parameters (e.g. significant wave height, Hs) are extracted from Wave Watch III® (WW3, Roland and Ardhuin, 2014) model simulations at the closest mesh point from the SCENES station. Hourly WW3 data are available from the MARC wave portal (https://marc.ifremer.fr). Wave statistics are calculated per tide to provide key metrics, such as the percentile 90 of significant wave height per tide (Hs_{P90}).

3.3. *SCENES station*

The SCENES station is part of the National Observation Service COAST-HF and the regional PHRESQUES monitoring network operating along the Seine River-Estuary-Bay continuum. It combines a surface buoy and a bottom station. The system was first deployed from January 2015 to June 2017, then slightly modified and redeployed from October 2017 until now (see details below, the dataset is open-access and available: see Verney et al., 2024).

3.3.1. Surface buoy

The surface buoy is instrumented with a CTD measuring salinity, temperature and dissolved oxygen; an optical turbidity and fluorescence sensor and a weather station. The CTD and optical sensors are both equipped with anti-fouling systems. CTD and optical sensors collect measurements between 1m and 1.5m below surface every 15min. Data are stored internally and available in real time using 4G transmission.

3.3.2. Bottom station

The bottom station is equipped with an Acoustic Doppler Profiler (ADP – Nortek AWAC), measuring the current velocity profile (first bin 1.4m above bed (mab), bin size 0.5m) and the acoustic backscatter profile, as well as wave parameters. Current measurements are collected every 30min, while wave measurements are collected every hour.

An optical sensor is also deployed from the bottom station. From 2015 to June 2017, only turbidity was recorded, 1.4mab. As the sensor was damaged by trawling, the optical sensor was then deployed 0.5mab from October 2017 and protected by a station frame. From 2017 to now, turbidity and fluorescence are recorded. Optical measurements are collected every 30min together with the current velocity profile.

3.4. Field campaigns

Regular field surveys were conducted close to the SCENES station approximately every 3 to 4 months when station sensors were replaced. Field surveys were conducted at least seasonally, except in 2016 when surveys were done every two months. Each survey consisted of at least one tidal cycle observation, and sometimes more. This results in a total of 47 tidal cycles, but only 19 complete cycles are available with the station fully operational.

3.5. Data processing

3.5.1. Processing field campaign observations

The same protocol was applied for all field campaigns and is fully described in Chapalain et al. (2019). Every 15min or 30min, CTD and optical sensor (OBS3+) profiles were realized. Data are collected at 4Hz and binned every 0.5m using downward cast. Every hour, subsurface and bottom water samples were collected using a horizontal Niskin bottle equipped with an optical turbidity and fluorescence sensor (identical to the optical sensor deployed from the station), allowing an optimal co-location of samples and optical measurements for NTU to SPMC calibration. Water samples were filtered on pre-ash, pre-weighted GFF filters, rinsed with demineralized water to remove remaining salts, air-dried at 50° for 24h and re-weighted to measure SPMC. The mean OBS3+ calibration coefficient is found to reach 0.00165g/l/NTU and is used in this study to calculate SPM concentration from the OBS3+.

3.5.2. Vertical bottom turbidity alignment between deployment periods

The elevation of the bottom turbidity measurements changed from the first deployment period (2015-June 2017; 1.4mab – $Turb_{1.4mab}$) to the second (Oct. 2017-now; 0.5mab – $Turb_{0.5mab}$). Data from the second period was therefore extrapolated to 1.4mab to provide a consistent SPMC signal from the acoustic backscatter data across the entire dataset. We calculated intratidal average turbidity climatology for each period (see section 3.5.5 for climatology calculation). All intratidal turbidity values for each condition of tidal range, wave intensity and river discharge from the two datasets are then compared using the ratio between $Turb_{1.4mab}$ and $Turb_{0.5mab}$ (Figure 2). Data are grouped by classes of climatology $Turb_{0.5mab}$ (every 10NTU from 0 to 100NTU, and one class from 100 to 200NTU), and corresponding ratio values are selected. For each class, the median and percentile 25 and 75 values are

calculated. Based on these statistical datasets, an empirical relationship comparing $Turb_{1.4mab}$ and $Turb_{0.5mab}$ is finally computed such as:

$$Turb_{1.4mab} = min\left(0.7 * e^{\frac{10-Turb_{0.5mab}}{40}} + 0.3; 1\right) * Turb_{0.5mab} \qquad \text{(Eq. 1)}$$

Hence for turbidity values at 0.5mab below 10NTU, no correction is applied, next the extrapolation factor exponentially decreases to reach 50% for $Turb_{0.5mab}$ around 50NTU and a plateau at 30% above 150NTU.

3.5.3. SCENES optical turbidity sensor calibration

All samples from field surveys are compared with optical turbidity measurements to evaluate an NTU to SPMC calibration function for sensors deployed on the station. No significant differences were observed between surface and bottom data, then all are pooled together. The calibration method developed by Landemaine (2016) and applied by Druine et al. (2018) and Chapalain et al. (2019) is used. The dataset (450 samples) is divided into 30 classes of 15 elements (division based on increasingly sorted turbidity values). Then in each class, one sample is randomly drawn and the linear relationship minimizing root-mean-square error (RMSE) is found. This is repeated 40000 times to get a stable probability density function of the calibration relationship. From this analysis, we observe that a range of calibration coefficients (from 0.0013 to 0.0018 g/l/NTU) corresponds to very similar RMSE. Then the median value within the lowest range of RMSE is used, i.e. 0.00156g/l/NTU. However, the SPMC was underestimated by ~0.001g/l for very low turbidity values. We decided to apply an offset of 0.001g/l to the calibration function:

$$SPMC = 0.00156 * NTU + 0.001 \qquad \text{(Eq. 2)}$$

Hence, even if the RMSE on the global dataset remain unchanged, bias and RMSE on the lowest SPMC are reduced. Finally, considering the calibration function described above, bias per concentration classes is below 15% and RMSE below 50%. We can also note that 70% of samples fall between calibration coefficients 0.0013 to 0.0025, which informs about the overall uncertainty when calibrating SCENES optical sensors over long time periods.

3.5.4. Evaluating bottom SPMC from ADP backscatter data

During stormy periods, the turbidity sensor at 0.5mab often saturated as turbidity exceeded 180NTU. To evaluate SPMC during this saturation regime, the acoustic backscatter signal can be calibrated and used. Moreover, inverting acoustic signal to SPMC over the whole water column is necessary to evaluate sediment fluxes. The acoustic inversion approach for calculating bottom SPMC is fully detailed in appendix 10.1, and is only briefly summarized below.

The Sonar equation is used to convert the raw acoustic backscatter into decibels and correct it for geometric and near-field corrections, spherical spreading and water attenuation, as detailed in Tessier et al. (2008) and Fettweis et al. (2019). The acoustic model developed by Thorne et al. (2014) is used to evaluate the calibration factor as a function of an optimal acoustic diameter, based on unsaturated bottom optical SPMC. This tidal optimal acoustic diameter is then averaged per tidal range and wave conditions, generating a tidal $D50_{opt\text{-}acc}$ climatology. This climatology can be used directly or dynamically-adapted to calculate optimal-acoustic SPMC ($SPMC_{opt\text{-}acc}$). $SPMC_{opt\text{-}acc}$ are substituted for the saturated optical SPMC measurements to create the final bottom SPMC time series.

3.5.5. Calculating intratidal statistical parameters at tidal scale for Hs, salinity, SPMC and SPM fluxes

Hs, surface salinity and surface and bottom SPMC time series are processed to evaluate intratidal and statistical parameters at the tidal scale. The original time series for each parameter is separated tide by tide, between two following low tides. The mean and percentiles 10, 50 and 90 are calculated for each tidal cycle.

Also, each tide is characterized by its tidal range, the Seine River discharge and the percentile 90 of Hs over the 3 previous tides. For each forcing, different classes are given: from 2 to 8m, every 1m or 0.5 for tidal range, five Q ranges ([0-300]; [300-500]; [500-700]; [700-1000]; [1000-2500]m^3/s) and five Hs_{P90} classes ([0-0.5]; [0.5-1.0]; [1.0-1.5]; [1.5-2]; [2.0-2.5]m). For each class of combined forcings, corresponding intratidal time series of surface or bottom parameters (i.e. SPMC) are interpolated on a common time array from low tide to low tide and are averaged, producing an intratidal climatology as shown later in Figure 10.

4. Results

4.1. Forcings, surface salinity and SPM dynamics

The Seine River discharge shows strong inter-annual variability from 2015 to 2022. Winter 2016-2017, 2018-2019 and 2021-2022 are characterized by low river inputs, rarely and very exceptionally exceeding 1000m^3/s (Figure 3). In 2019-2020 and 2020-2021, the river discharge follows the average dynamics, with high values (exceeding 1800m^3/s) in January-February. Year 2015-016 is particular as an exceptional flood was recorded in June, reaching 2000m^3/s while on average a discharge of 400m^3/s is usually expected at this period of the year. Winter 2017-2018 was also particular, with an intense and remarkably long flood event: the river discharge was continuously above 1000m^3/s from January to April 2018.

The wave activity also follows a well-identified seasonal dynamics, with storms mainly occurring from October to March. During this period, storms induce Hs_{P90} ranging from 1 to 2m. Strongest

events reach Hs_{P90} value above 3m. Winter 2017-2018, 2019-2020 and 2021-2022 are the most intense periods.

Surface salinity ranges from 10 to 34 PSU at the interannual scale, and as the river discharge shows a strong seasonal variability, with lower salinity (~20PSU) during high river flow (>1000m^3/s). At the tidal scale (not shown), surface salinity is lower during ebb and around slack, when ebb currents flush out estuarine brackish water towards the bay.

Surface and bottom SPMC significantly varies seasonally in response to forcings (Figure 3). In general, SPMC at surface and bottom are the highest during winter, ranging from 0.01 to 0.1g/l at surface and from 0.01 to 1g/l at 1.4mab. SPMC decreases seasonally from spring to summer, together with lower wave conditions. At the end of summer, surface SPMC ranges from 0.005 to 0.02g/l and bottom SPMC from 0.005 to 0.08g/l. Tides also affect the SPMC variability, but this effect is not easily visible at the interannual scale. It can be observed during summer, in absence of wave and when tides dominate the hydrodynamic forcing, a neap-spring variability of the tidal-median SPMC, especially close to the bed. Further investigations on the influence of each forcings on SPMC dynamics are explored in the discussion section.

Depth-average current velocity (Figure 4) also significantly changes at the tidal scale. Peak flood currents are the strongest 1h to 2h after low tide and are directed southeast, following the estuary mouth funnel shape. Next, the current direction turns northward between 3h after low tide and high tide, due to tide propagation into the English Channel, generating a strong northward current, and named locally as the Verhaule current. Ebb currents are the strongest 2h to 3h after high tide and orientated north-west to west. Current intensity generally increases with the tidal range, with peak flood currents ranging on average from 0.2m/s during neap tides to 0.9m/s during spring tides.

4.2. Examining density circulation at the estuary mouth

At the estuary mouth, estuarine hydrodynamics and sediment transport are mainly controlled by tidal current (and tidal pumping) and density circulation. The latter is driven by confronting marine waters and riverine freshwaters, and the resulting vertical and horizontal gradients. While tidal pumping is clearly observed from current ellipses (Figure 4), with peak flood barotropic velocities during flood twice larger than the ebb velocities, and larger SPMC during flood, examining density circulation intensity requires further analysis.

The vertical salinity gradient will be evaluated first. As bottom salinity is not recorded at the SCENES station, bottom salinity was explored from CTD field surveys. Bottom salinity was shown to weakly vary between 31.5 and 33.5, and therefore fixed to a mean constant value of 32.5 PSU. The salinity gradient was then calculated by subtracting the mean bottom salinity from the recorded surface salinity. In this way, the salinity gradient per tidal range and river discharge conditions was calculated (for low wave conditions - Figure 5). As expected, the salinity gradient decreases with increasing tidal ranges (tidal mixing) and increases with increasing river discharge. For low river flow conditions ($Q<300m^3/s$), the vertical salinity gradient varies from -1.5 PSU (spring tide) to -4.5 PSU (neap tide), while it ranges from -5 PSU (spring) to -12 PSU (neap) for Q values above $1000m^3/s$.

The mean bottom velocities (averaged on the 9 first bins above the bed, i.e. from 1.4 to 4.9m) were extracted from the ADP dataset, and residual velocities were calculated for low wave conditions. These residual bottom velocities are averaged by tidal range and river discharge classes (Figure 5). For low to moderate river flow conditions, residual velocities are the strongest for low to moderate tidal ranges, reaching 0.02m/s and directed upward, while the highest spring tides are associated with seaward residual flows (around -0.02m/s). As observed in Figure 3 and Figure 5, increasing river flow yields to a decrease in surface salinity, hence enhancing stratification and density circulation: higher river flows and enhanced stratification lead to increase the landward residual bottom velocities (for low tidal range) and to turn residual flow direction during spring tides: for tidal range between 6m to 7m, the bottom residual velocities for low river flow ($Q<300m^3/s$) reaches -0.025m/s (seaward), while for high to exceptional river flows ($Q>500m^3/s$) residual velocities are positive (upward) and reach

0.01m/s and 0.02m/s respectively. For moderate tidal ranges, bottom residual velocity values are stronger and range from 0.02 to 0.06m/s. These observations are in good agreement with model results of Schulz et al. (2018) at a similar location in the estuary.

4.3. *SPM fluxes*

4.3.1. *Evaluating SPM fluxes*

Surface and bottom SPM fluxes are calculated from surface and bottom SPMC and current velocity (bin 1.5m below surface and 1st bin above the bed respectively). Calculating depth-integrated SPM fluxes is more challenging, as it requires evaluating SPMC over the whole water column using the acoustic backscatter signal (Eq. 3). Similarly to acoustic bottom concentration (3.5.4.), the main issue is to evaluate the vertical and temporal D50 variability, essential for the acoustic inversion. Bottom and surface SPMC time series can be used to evaluate bottom and surface optimal D50, but evaluating D50 for all bins in the water column requires an extrapolation method. This method is fully detailed in appendix 10.2.

The SPM concentration at all times and all bins in the water column computed from ADP backscatter data can be compared with ship-based (OBS-derived) SPMC measurements (Figure 6). Calculated ADP SPMC data are in good agreement with ship-based SPMC, with median values per SPMC class less than 10% different from the reference, and percentile 25 and 75 always within the +/-50% interval. The largest differences are observed below 0.003g/l (overestimation) and over 0.07g/l (underestimation by 20% to 40%).

SPM depth-integrated fluxes are computed using ADP SPMC and current velocity profiles, projected along the main flood current direction (see dashed line in Figure 4). However, ADP bins do not cover the whole water column, due to blind areas near the transducers (bin 1 is 1.4mab) and approximately 1m below surface. SPM fluxes at bin 1 are extended from the seabed to bin 1. SPM fluxes measured

1.5m below surface are also extended to the sea surface, hence providing fluxes over the whole water column. Intratidal depth-integrated fluxes, surface and bottom fluxes are integrated over each tide to calculate respective residual fluxes.

4.3.2. SPM fluxes time series

SPM fluxes dynamics are illustrated for two contrasted meteorological conditions, i.e. for calm weather (Hs_{P90}<1m - Figure 7) and storm conditions (Hs_{P90}>2m - Figure 8).

During calm weather conditions, bottom, surface and depth-integrated fluxes increase with tidal range, as more energetic conditions are associated with stronger current velocities and larger SPMC in the water column. Bottom fluxes are stronger than surface fluxes independent of tidal range. Maximum bottom fluxes values were observed during flood phase, ranging from 0.008kg/m/s during neap tide (TR=3.8m) to 0.015 kg/m/s during moderate spring tide (TR=5.5m). During flood phase, surface fluxes reach 0.002 to 0.004 kg/m/s from neap to spring. During ebb, bottom and surface fluxes show similar values, ranging between 0.002kg/m/s to 0.004kg/m/s. Sheared fluxes are observed around low tide, with positive (up river) bottom fluxes and negative (seaward) surface fluxes.

Depth-integrated fluxes show similar behaviour as the sum of the surface and bottom fluxes, with increasing strong upward flood fluxes reaching 0.25kg/m/s during spring tide, and less than 0.1kg/m/s during neap tide.

Residual bottom fluxes are significantly larger than residual surface fluxes, and residual depth-integrated fluxes are all positive, indicating that sediment is being imported to the estuary from the sea. The depth-integrated residual fluxes increase with tidal range, varying from 400 kg/m per tide for low tidal ranges to 800 kg/m per tide for moderate tidal ranges.

The general dynamics described above change considerably during storm conditions (Figure 8). Moderate wave conditions (1m<Hs<2m – 01/10-01/12) show larger bottom fluxes compared with surface fluxes during the flood phase, but depth-integrated flux intensities are similar during ebb and

flood (around 0.1kg/m/s). From the 13th to 14th of January, Hs values are larger than 2m and reach up to 3m. Surface and bottom fluxes strongly increase, reaching 0.03 kg/m/s and 0.1 kg/m/s respectively. These values are 4 to 6 times larger than during calm conditions. Depth-integrated fluxes also increase during storms, e.g. up to 2kg/m/s during flood and -2kg/m/s during ebb. These intense resuspension conditions, associated with strong mixing due to high tidal range (TR>6m) yield strongly negative seaward fluxes, both observed from raw and residual depth-integrated fluxes, often reaching -2000 to -5000 kg/m per tide. While Hs decreases (Hs<1m – 16/01/2017), residual depth-integrated fluxes still show negative values, highlighting an hysteresis-time lag effect on SPMC before before the system returns to normal (calm) condition, up to 2 tides after strong wave condition (17/01/2017).

5. Discussion

5.1. Unravelling the impact of tides, waves and river discharge on SPM concentration

5.1.1. Q/TR/HS on SPM concentration

Tide, river discharge and storms play a significant role on the SPMC patterns throughout the year, but highlighting and unravelling their individual contribution is challenging, because the forcings are often superimposed. A first approach is to analyse the tidal-median SPMC variability per conditions of tidal range, river discharge and wave activity (Figure 9).

Surface and bottom tidal-median SPMC show similar trends, but different orders of magnitude, with higher SPMC being observed near the bottom. For a given river flow condition, the tidal-median SPMC increases with the tidal range. For instance, for average river flow conditions (300-500m^3/s) and low wave activity (Hs_{P90}<1m), tidal-median surface SPMC increases from 0.008g/l to 0.010g/l while tidal-median bottom SPMC ranges from 0.015 to 0.035g/l.

Increasing river discharge causes an increase in both surface and bottom SPMC, with a factor from 2 to 3. Hence, for tidal range values between 3 and 4m, median tidal-median surface SPMC increases from 0.005 to 0.013g/l and bottom values from 0.009 to 0.02g/l.

Wave events significantly increase SPMC, and the stronger the wave event, the higher the SPMC. Figure 9 shows the impact of waves (Hs_{P90}=[1-2]m and Hs_{P90}=[2-3]m) for river discharge ranging from 300 to 500m^3/s. This effect is observed both for surface and bottom, but is larger near the bed, with median tidal-median concentration ranging from 0.04 to 0.08g/l for Hs_{P90} values above 2m. For a given tidal range condition, the variability in bottom tidal-median SPMC induced by wave events is large, ranging from 0.025 up to 0.2g/l.

5.1.2. Intratidal SPMC Climatology

As observed above, the SPMC tidal signal is strongly entangled with the contribution of wave and river discharge. In order to separate the tidal contribution from the raw high-frequency signal, an SPMC climatology, i.e. an intratidal-average signal, is computed from the raw data, representative of low wave (Hs_{P90}<1m) and mean river discharge (Q=[300-500]m^3/s) conditions. First, all tides corresponding to these criteria are extracted. Then selected tides are separated by tidal range (from 2 to 8m, every 1m) and tidal range gradient conditions (positive: neap to spring; negative: spring to neap) (refer to section 3.5.5. for the description of the methodology).

Contrary to median tidal SPMC patterns, which are similar for surface and bottom SPMC (see section above), intratidal SPMC patterns highlight the influence of the main forcing on the respective dynamics (Figure 10). Surface SPMC values are the highest around low tide, associated with low salinity conditions, while the lowest SPMC values are found around high tide (around 0.01g/l on average). This pattern is clearly visible from mid to high tidal ranges (TR>4m), and the magnitude of

the maximum SPMC value around low tide increases with the tidal range, from 0.015g/l for TR values between 5 to 6m up to 0.035g/l for TR values above 7m.

Bottom concentration follows a different pattern, with the highest SPMC observed 1h to 3h after low tide, during the flood phase. At the end of the flood phase, 4h to 5h after low tide, a second peak in SPMC can be observed associated with the Verhaule northward current, on average 20% lower than the main flood peak and advecting sediment from the main channel. Then SPMC decreases progressively until high tide and remains stable or weakly increases during the ebb phase. Similarly to surface SPMC, the magnitude of the bottom SPMC signal is correlated with the tidal range, the maximum bottom SPMC reaching 0.065g/l during high spring tide (TR>7m), and reaching still nearly 0.03g/l for low to moderate tidal ranges (TR =[4-5]m). Bottom SPMC during ebb is also modulated by the tidal range, ranging from 0.01g/l during the lowest neap tides to 0.03g/l during the highest spring tides.

Differences between fortnightly tidal phases are low for high tidal ranges, but more significant for neap tides, especially near the bed. For tidal ranges between 4 to 5m, peak SPMC during the flood is 30% larger from spring to neap than neap to spring (increasing from 0.028 to 0.037g/l). Similarly, the SPMC during ebb is larger, increasing from 0.01 to nearly 0.02g/l from positive to negative tidal range gradient, respectively.

These differences in SPMC patterns are related to different dominant processes for surface and bottom concentration. Bottom SPMC dynamics is driven by local resuspension, especially during flood phase when peak current velocity can reach up to 1m/s. Bottom sediments resuspended by tidal currents seem to weakly reach the surface. High SPMC around low tide is related to estuarine brackish water being flushed out the estuary towards the bay at the end of ebb tide and around low tide. The increase in SPMC with the tidal range is driven by ETM resuspension in the estuary and advected toward the mouth during ebb.

5.1.3. SPM concentration anomalies

The intratidal SPMC signal can then be used to evaluate the contribution of wave events and river discharge by analysing SPMC anomalies (i.e. subtracting the intratidal signal from the raw signal) (Figure 11). Both surface and bottom SPMC anomalies vary around 0, but anomalies are mainly positive. High positive surface SPMC anomalies (above 0.05g/l and up to 0.1g/l) are observed during intense wave events, and correspond to twice the maximum tidal-induced SPMC observed during spring tide. The role of river discharge is more difficult to evaluate from time series. Negative anomalies (around 0.01g/l maximum) are mainly observed during summer, when the river discharge is the lowest.

Bottom SPMC anomalies range between 0.05 and 0.5g/l, and are often associated with intense wave events, as observed at the surface. These positive anomalies can reach up to 10 times the maximum tidal-induced concentration during spring tide (Figure 10). Similarly to surface SPMC, negative anomalies are observed during summer and low river discharge conditions.

Tidal-median SPMC anomalies are computed and separated by Hs_{P90} and river discharge conditions to further investigate the relative influence of river discharge and wave events on SPMC anomalies, similarly to results shown in section 5.1.1. In agreement with Poppeschi et al. (submitted), Figure 12 confirms the dominant role of wave events on suspended sediment dynamics at the mouth of the estuary, with median anomalies during intense wave events that can reach 4 times the tidal median SPMC during spring tide, i.e. 0.1g/l. More interestingly, this figure highlights the weaker but noticeable influence of the river discharge. In absence of wave (Hs_{P90}<1m) bottom and surface anomalies increase with river discharge, reaching 0.01 g/l and 0.005 g/l respectively during intense flood events (Q>1000m^3/s). This contribution for high river discharge is on average equivalent to the tidal contribution. The influence of river discharge is also observed during moderate storms (Hs_{P90}<2m), though the signal is not as clear as in absence of wave.

While the influence of wave events is associated with "local" resuspension (i.e. at the mouth), the contribution of river discharge is directly related to ETM dynamics. With increasing river discharge, the ETM is progressively shifted downstream until being centred nearly at the estuary mouth for large river discharge ($Q>1000m^3/s$) as shown by Grasso et al. (2018). This results in higher SPMC at the surface that arrives at the station sooner during the ebb phase due to enhanced vertical stratification. The seaward movement of the ETM also provides an additional source of easily fresh erodible sediments by tidal currents and waves on the seafloor. On the contrary, low river discharges ($Q<300m^3/s$) and calm weather periods are associated with an upward shift of the ETM and less sediment available for resuspension or advection at the mouth and result in weak (~-0.005g/l) negative anomalies.

5.2. *Unravelling the impact of tides, waves and river discharge on residual SPM fluxes*

5.2.1. *Relative influence of forcings*

The influence of tides and waves on residual fluxes was illustrated in 4.3.2. and highlighted that, overall, calm conditions are associated with an import of SPM to the estuary mouth (modulated by tides), while stormy conditions lead to an export of SPM from the estuary to the bay. The relative contribution of forcings to residual SPM fluxes at the estuary-sea interface is further examined in this section, grouping residual fluxes values per conditions of wave, tidal range and river discharge and calculating median values, as presented in Figure 13.

Surface residual fluxes are generally negative (directed seaward), increase with tidal range (TR>6m) and wave intensity (Hs_{P90}>1.5m) and exceed 50kg/m per tide. Increasing river discharge weakly increases surface residual fluxes, despite an increase in SPMC concentration for high river flow as observed in Figure 9. This is because the increase in SPMC span +/-3h around LT, and positive early flood phase fluxes partly compensate negative ebb phase fluxes.

Bottom residual fluxes are directed landward, also increase with increasing tidal range, and show higher values during high wave conditions. The impact of increasing river discharge is even more significant, with a 2-fold increase especially for moderate to high tidal range conditions (4m<TR<7m). This is first explained by higher and asymmetric SPMC during high river flow, proportionally larger during flood than ebb, due to the ETM shift toward the mouth (Grasso et al., 2018). Also, high river flow enhances vertical and longitudinal stratification at the mouth and strengthens density circulation (Figure 5), leading to landward bottom sediment fluxes (Burchard and Baumert, 1998; Diaz et al., 2020; Grasso et al., 2021; Grasso and Le Hir, 2019; Schulz et al., 2018).

Considering depth-integrated residual fluxes and low to moderate river discharge ($Q<500m^3/s$), sediments are globally imported to the estuary for low to moderate tidal ranges (TR<6) and low wave conditions ($Hs_{P90}<1.5$), and exported to the sea for high tidal range conditions and storm events (TR>6m or $Hs_{P90}>1.5m$), due to stronger mixing in the water column during both flood and ebb as observed by Sommerfield and Wong (2011) in the most downstream part of the Delaware Estuary. The export of sediments during wave events was also observed by Figueroa et al. (2020), although weaker as their study site was more protected from waves than the Seine mouth. High and exceptional river discharge ($>500m^3/s$) are associated with positive (landward) and higher residual fluxes, even for high tidal range or wave conditions, related to the significant increase in near-bottom density circulation (Figure 5). This competition between tidal pumping, stratification and density circulation was already pointed out by McSweeney et al. (2016).

The comparison of the Seine dynamics with previous studies is not straightforward as most prior observations mainly focused on ETM dynamics, or in regions with different settings in terms of SPMC, width and depth, and wave influence. However, results can be compared with numerical simulations from Schulz et al. (2018) and Grasso et al. (2021) in the Seine Estuary. Schulz et al. (2018) subdivided the estuary mouth into boxes and calculated fluxes at all boundaries, and along full cross-sections from south to north, one offshore, common with Grasso et al. (2021) and one close to the mouth. The comparison between model and observations can only be qualitative as models

integrate fluxes over segments or cross-sections while observations are local and not representative of the full cross-section exchange, with potential cross-estuary shear fluxes as illustrated by McSweeney et al. (2016). In addition, Diaz et al. (2020) show that simulated fluxes between estuaries and coastal seas are associated with large uncertainties due to the equifinality effects in sediment transport parameterisation. Observations and model results agree on the general patterns, i.e. landward residual fluxes increasing with tidal range, the export of sediment during storms and the import of sediment with increasing river discharge. Model results do not clearly show the inversion of residual fluxes seaward when tidal ranges exceed 6m for low wave conditions, but the simulation analysis did not separate results by wave conditions, which precludes direct comparisons.

Complementary cross-estuary observation at the mouth should be prioritized in the near future to improve sediment exchange understanding at the interface between the estuary and the coastal sea, and examine the interaction between the morphology of the mouth and sediment fluxes.

5.2.2. Residual fluxes: uncertainty and limitations

These median (or mean) residual fluxes $F_{res,50}$ values are associated with uncertainty estimation U_F (triangles in Figure 13), representing the spread of residual fluxes per forcing conditions. A given condition is flagged uncertain if the median residual flux is positive (negative) and the percentile 25 (75) is negative (positive). The intensity of the uncertainty is quantified as:

$$\begin{cases} U_F = \left| \dfrac{F_{res,50} - F_{res,25}}{F_{res,50}} \right| & if\ F_{res,50} > 0 \\ U_F = \left| \dfrac{-F_{res,50} + F_{res,75}}{F_{res,50}} \right| & if\ F_{res,50} < 0 \end{cases}$$

For forcing conditions at the interface between landward to seaward fluxes, U_F is the largest, meaning that raw residual fluxes can also be directed opposite to the median flux direction. Hence these forcing conditions represent transitional patterns. This uncertainty can be caused by: i) possible miscalculation of SPMC vertical profiles, mainly during wave events where the ADP calibration vertical extrapolation

can be questioned as not validated by ship-based surveys; and ii) the low occurrence of observations for these hydro-meteorological conditions hence weakening the statistical significance. This demonstrates that maintaining coastal and estuarine observatories and improving the continuity in measurements for long-term periods (i.e. decades) is essential to consolidate our understanding of SPM dynamics and SPM fluxes in these critical and complex areas.

A weakness in the current dataset is gaps in surface or bottom data, sometimes for very long time periods such as in 2019-2020 for surface data. Integrating *in situ* observations and ocean colour satellite data based on the most recent algorithms could provide a relevant solution for filling gaps and extending the surface dataset (Ody et al., 2022; Tavora et al., 2020). Similarly, statistical and machine learning gap-filling techniques (Arriagada et al., 2021; Phan et al., 2020) could also be carefully explored to densify observations.

5.2.3. An attempt for calculating annual cumulative residual fluxes and sediment budget

Extending investigations to evaluate cumulative fluxes and hence analyse annual to pluriannual SPM exchange at the mouth of the estuary is more challenging. Observations in the present study are not continuous in time, and cannot be directly used to reach this objective. Median depth-integrated residual fluxes shown in Figure 13 can first be used, constituting residual fluxes times series by associating the median residual flux to the corresponding forcing conditions (Figure 14), tide by tide. This approach concludes with a long-term sediment import to the estuary (+300ton/m over 7 years), which is not in agreement with Schulz et al. (2018), who find that this area mainly exports SPM. In this approach, calculating median fluxes per condition biases the results for conditions weakly observed (less than 10 tides from 2015 to 2022) and when raw fluxes values show strong and asymmetric (positive/negative) variability. Indeed, flux values are highly scattered when analysing the whole dataset, with far larger negative values than positive values. Then, using a median operator smooths these high negative values, and biases results toward positive, importing, fluxes. Using the

mean operator instead also biases results but in the opposite direction: the mean operator gives more weight to extremely negative values. Hence cumulative fluxes calculated from mean flux values conclude to strong negative, exporting, fluxes (-250ton/m) in 7 years. If the flux direction is now in line with model results on the area obtained by Schulz et al. (2018), the cumulative flux intensity is also questionable, as most high energetic conditions are rarely observed in our dataset, and statistics might not be reliable. Increasing the amount of collected data with coming observations in the next year will certainly improve statistics reliability, and hence cumulative flux estimation, but a new approach can also be tested with the existing dataset.

It should be noted that, as observed Figure 13, using mean or median operators does not change the conclusions on the role of forcings on residual fluxes when forcing intensities are low to moderate. The impact is mainly visible for high wave conditions and high tidal ranges that were already flagged as uncertain, and for which mean or median values change from positive to negative or show strong negative values.

Considering the previous methods unsatisfactory, a new method directly using the probability density function (PDF) of observed fluxes per condition can be used, hence accounting for intra-condition residual fluxes scattering. For each tide, a residual flux is randomly drawn within the PDF corresponding to the tidal condition. The more frequent the flux value, the higher the probability of getting this value. This stochastic approach is repeated 300 times to create a consistent ensemble of possible cumulative residual fluxes (Figure 14), and the ensemble average is calculated. This approach also informs about the uncertainty in cumulative flux estimation. Cumulative residual fluxes calculated at the end of the study period range from weakly importing values (+50ton/m) to high exporting values (-200ton/m). The ensemble average residual flux reaches -80ton/m, far from the mean export value exceeding -250ton/m.

Annual local sediment budgets can also be estimated by separating each year (from October to October) and calculating annual cumulative residual fluxes, and compared with wave and river

discharge annual statistics (Figure 15). Wet years (average Q>500m^3/s) mainly show positive residual fluxes. Year 2015-2016 show the highest positive residual flux as it combines annual high river discharge and low wave conditions. Year 2019-2020 is the stormiest year, and sediment budget is the most negative, exporting sediment. Other years highlight the competition between wave-driven export and density circulation-driven import. When annual wave conditions are similar, increasing river discharge lead to significant exportation reduction, and even, for the largest river discharge, to sediment import conditions. Year 2016-2017 is atypical because it is characterized by the lowest wave conditions, but is also one of the most exporting years. This may be explained by exceptionally low river discharge conditions, hence weakening the density circulation contribution, and increasing the relative contribution of tidal-driven fluxes or wave-driven fluxes.

This method to evaluate sediment budgets shows promising results, but must be strengthened by i) increasing the length of the dataset; ii) improving measurement continuity; iii) consolidating SPM concentration calculation from ADP measurements during storm conditions.

5.3. Combining acoustics and optics: insights about SPM composition

Most studies using ADP to estimate vertical SPM concentration profile use an empirical linear relationship between the acoustic backscatter index BI and $\log_{10}$ of the SPM concentration (Dufois, 2014; Fettweis et al., 2019; Figueroa et al., 2020; McSweeney et al., 2016; Tessier et al., 2008). This method is convenient and easy to implement, but can show limitations for long-term deployments as calibration should be regularly updated. Moreover, as slope coefficient can significantly move far from 1 for each calibration, hence diverging from theory, these coefficients cannot be related to any physical SPM feature.

The approach developed in this study follows theoretical developments (Thorne et al., 2014), calculating an equivalent optimal acoustic diameter $D50_{opt\text{-}acc}$ for each acoustic profile. This $D50_{opt\text{-}acc}$ was first considered as a calibration parameter, but it could also be, with care, considered as qualitatively characterizing the near bed SPM composition, in terms of sand-mud content, as explored by Pearson et al. (2021) with the Sediment Composition Index (SCI). By analogy with their study, SCI is equivalent to $-f(D50_{opt\text{-}acc})=-10\log10(s/(r*v))$ in Eq. 4; then when $D50_{opt\text{-}acc}$ increases, SCI decreases and sand content increases. However, the absolute $D50_{opt\text{-}acc}$ value calculated by the inversion algorithm cannot be considered as representative of the median SPM particle size, but only as a proxy for sand or mud content. Indeed, the acoustic backscatter intensity has not been fully calibrated, and the system constant still needs to be estimated. This absolute calibration requires further investigations and accurate knowledge on particles and/or flocs in suspension, which is out of the scope of this study.

Examining raw $D50_{opt\text{-}acc}$ time-series (Figure 16) and intratidal average $D50_{opt\text{-}acc}$ (Figure 17) illustrates the sand/mud content variability in response to tidal and wave forcing: low $D50_{opt\text{-}acc}$ values are observed during neap tides and around slacks at the tidal scale; and high values are found during spring tides and during flood phase at the tidal scale. For increasing tidal ranges, $D50_{opt\text{-}acc}$ increases during flood phase with an abrupt increase for the largest tidal range values, indicating a non-linear increase in sand content with tidal range. This is in agreement with literature and theory: current velocity increases and turbulence conditions are likely to erode and resuspend fine sand in suspension, and sand erosion fluxes are non-linearly correlated with current velocity (Soulsby, 1997). This would suggest a net import of sand toward the estuary. We can also note if waves on average are associated with higher $D50_{opt\text{-}acc}$ values (Figure 17), intense wave events do not always necessarily correspond to high $D50_{opt\text{-}acc}$ values (Figure 16). This might be explained by either uncertainty in the extrapolation of the near-bed SPMC to observation 1.4mab, or due to incomplete sediment attenuation correction.

Two populations of particles, sand grains and flocs, are assumed to be possibly found in suspension. It could be envisaged to process the acoustic inversion considering a bimodal sand/floc population, expanding from the work by Fromant et al. (2017) on flocs and using the coupled optical-acoustic

sensors to evaluate sand/mud fraction and total concentration. Investigating further acoustic inversion, including accurate absolute instrument calibration and bimodal SPM population may improve our understanding of the SPM composition and hence the quantification of both sand and mud concentrations and fluxes.

6. Conclusions

In situ high-frequency optical and acoustic observations were analysed to evaluate suspended particulate matter concentration at the surface and near the bed. An iterative inversion technique was applied to calibrate long-term acoustic measurements using equivalent D50. A climatology of equivalent D50 was computed as a function of intratidal and subtidal dynamics, highlighting the probability for sand particles to be resuspended during spring tide flood phases, and during wave events. An original method was proposed to extrapolate equivalent D50 along the water column from surface and bottom measurements and hence calculating SPM concentration everywhere in the water column and reducing uncertainty. Further developments on acoustic inversion including two populations of particles could be further investigated to potentially evaluate both sand and fine sediment in suspension.

Surface and bottom measurements were examined to evaluate hydrodynamics, SPM dynamics and exchange between estuary and coastal sea in response to tides, river discharge and waves. Surface dynamics was shown to be correlated with the tidal range, the river discharge and waves. Surface SPM concentrations during spring are twice the SPM concentrations observed during neap. For a given tidal range, increasing river discharge leads to increase SPM concentrations by a factor of 2 due to the shift of the estuarine turbidity maximum toward the mouth, and high waves again multiply by 2 SPM concentrations for a given tidal range and river discharge. At tidal scale, the same patterns are observed near the bottom, while SPM concentrations are on average twice the surface SPM

concentrations. Moreover, the impact of storms on bottom SPM concentrations is more significant. These results highlight the cumulative impact of tidal and hydro-meteorological forcings on SPM concentration. The tidal-induced SPM concentration can possibly hide the impact of other forcings, hence an intratidal climatology of SPM concentration for low-wave conditions and mean river discharge ($300<Q<500 m^3/s$) was calculated for TR classes. Subtracting this climatology to high-frequency raw signal yields to evaluate SPM concentration anomalies, emphasizing the role of waves and river discharge.

Surface, bottom and depth-integrated SPM fluxes were evaluated, and residual fluxes were analysed by forcing conditions. Residual fluxes are directed upward, importing sediment to the estuary for moderate tidal ranges (TR=[3 6]m) and low wave conditions. For high tidal range, residual fluxes are directed seaward, due to higher SPM concentration along the tidal cycle. Waves and tides contribute to higher SPM concentration in the water column and hence residual fluxes are oriented seaward. In case of high and exceptional river discharge ($Q>500 m^3/s$), the density circulation is strengthened and induces stronger importing residual fluxes, even for high tidal ranges.

These analyses can be further compared with modelled fluxes to contribute to consolidating model calibration and reducing uncertainty. These results from long-term observation strategy are also valuable to evaluate future changes in sediment exchange at the interface between estuary and coastal sea induced by estuarine management and climate change.

7. Open data

All data used in this manuscript are publicly available. Part of these data are already available on: https://coast-hf.fr/. SCENES data are available here: https://doi.org/10.17882/99434 (Verney et al., 2024).

8. Acknowledgments

This work was co-funded by Ifremer and the PHRESQUES project, coordinated by the GIP Seine Aval. PHRESQUES was funded by the CPIER « Vallée de Seine », the Seine Normandy Water Agency (AESN), and the Normandie and Ile de France Regions. This project is also supported by the eLTER « Zone Atelier Seine » . This study also contributes to the RUNTIME project, co-funded by the EC2CO program and OFB.

We would like to acknowledge the COAST-HF (http://www.coast-hf.fr) national observing network component of the National Research Infrastructure ILICO, as well as the CNFC and RV Thalia and Côtes de la Manche crews for their support in field surveys.

9. References

Arriagada, P., Karelovic, B., Link, O., 2021. Automatic gap-filling of daily streamflow time series in data-scarce regions using a machine learning algorithm. Journal of Hydrology 598, 126454. https://doi.org/10.1016/j.jhydrol.2021.126454

Artelia, 2019. Définition des périodes de retour des forçages et des niveaux de pleines mers en estuaire de Seine pour la gestion du risque inondation.

Avoine, J., 1981. L'estuaire de la Seine : sédiments et dynamique sédimentaire. Caen University.

Avoine, J., Allen, G.P., Nichols, M., Salomon, J.C., Larsonneur, C., 1981. Suspended-sediment transport in the Seine estuary, France: Effect of man-made modifications on estuary—shelf sedimentology. Marine Geology 40, 119–137. https://doi.org/10.1016/0025-3227(81)90046-3

Brenon, I., Le Hir, P., 1999. Modelling the Turbidity Maximum in the Seine Estuary (France): Identification of Formation Processes. Estuarine, Coastal and Shelf Science 49, 525–544. https://doi.org/10.1006/ecss.1999.0514

Burchard, H., Baumert, H., 1998. The Formation of Estuarine Turbidity Maxima Due to Density Effects in the Salt Wedge. A Hydrodynamic Process Study. Journal of Physical Oceanography 28, 309–321. https://doi.org/10.1175/1520-0485(1998)028<0309:TFOETM>2.0.CO;2

Burchard, H., Schuttelaars, H.M., Ralston, D.K., 2018. Sediment Trapping in Estuaries. Annu. Rev. Mar. Sci. 10, 371–395. https://doi.org/10.1146/annurev-marine-010816-060535

Chapalain, M., Verney, R., Fettweis, M., Jacquet, M., Le Berre, D., Le Hir, P., 2019. Investigating suspended particulate matter in coastal waters using the fractal theory. Ocean Dynamics 69, 59–81. https://doi.org/10.1007/s10236-018-1229-6

Cloern, J.E., 1987. Turbidity as a control on phytoplankton biomass and productivity in estuaries. Continental Shelf Research 7, 1367–1381. https://doi.org/10.1016/0278-4343(87)90042-2

Costanza, R., d'Arge, R., de Groot, R., Farber, S., Grasso, M., Hannon, B., Limburg, K., Naeem, S., O'Neill, R.V., Paruelo, J., Raskin, R.G., Sutton, P., van den Belt, M., 1997. The value of the world's ecosystem services and natural capital. Nature 387, 253–260. https://doi.org/10.1038/387253a0

Cox, J.R., Dunn, F.E., Nienhuis, J.H., van der Perk, M., Kleinhans, M.G., 2021. Climate change and human influences on sediment fluxes and the sediment budget of an urban delta: the example of the lower Rhine–Meuse delta distributary network. Anthropocene Coasts 4, 251–280. https://doi.org/10.1139/anc-2021-0003

Cuvilliez, A., Deloffre, J., Lafite, R., Bessineton, C., 2009. Morphological responses of an estuarine intertidal mudflat to constructions since 1978 to 2005: The Seine estuary (France). Geomorphology 104, 165–174. https://doi.org/10.1016/j.geomorph.2008.08.010

Deloffre, J., Lafite, R., Lesueur, P., Verney, R., Lesourd, S., Cuvilliez, A., Taylor, J., 2006. Controlling factors of rhythmic sedimentation processes on an intertidal estuarine mudflat — Role of the turbidity maximum in the macrotidal Seine estuary, France. Marine Geology 235, 151–164. https://doi.org/10.1016/j.margeo.2006.10.011

Diaz, M., Thouvenin, B., Grasso, F., Le Hir, P., Sottolichio, A., Caillaud, M., 2020. Modeling mud and sand transfers between a macrotidal estuary and the continental shelf: influence of the sediment-transport parameterization. Journal Of Geophysical Research-oceans. https://doi.org/10.1029/2019JC015643

Druine, F., Verney, R., Deloffre, J., Lemoine, J.-P., Chapalain, M., Landemaine, V., Lafite, R., 2018. In situ high frequency long term measurements of suspended sediment concentration in turbid estuarine system (Seine Estuary, France): Optical turbidity sensors response to suspended sediment characteristics. Marine Geology 400, 24–37. https://doi.org/10.1016/j.margeo.2018.03.003

Dufois Francois, C.S., Verney Romaric, Le Hir Pierre, Dumas Franck, 2014. Impact of winter storms on sediment erosion in the Rhone River prodelta and fate of sediment in the Gulf of Lions (North Western Mediterranean Sea). Continental Shelf Research. https://doi.org/10.1016/j.csr.2013.11.004

Dunn, F.E., Darby, S.E., Nicholls, R.J., Cohen, S., Zarfl, C., Fekete, B.M., 2019. Projections of declining fluvial sediment delivery to major deltas worldwide in response to climate change and anthropogenic stress. Environmental Research Letters 14, 084034. https://doi.org/10.1088/1748-9326/ab304e

Etcheber, H., Schmidt, S., Sottolichio, A., Maneux, E., Chabaux, G., Escalier, J.-M., Wennekes, H., Derriennic, H., Schmeltz, M., Quéméner, L., Repecaud, M., Woerther, P., Castaing, P., 2011. Monitoring water quality in estuarine environments: lessons from the MAGEST monitoring program in the Gironde fluvial-estuarine system. Hydrology and Earth System Sciences 15, 831–840. https://doi.org/10.5194/hess-15-831-2011

Fettweis, M., Riethmüller, R., Verney, R., Becker, M., Backers, J., Baeye, M., Chapalain, M., Claeys, S., Claus, J., Cox, T., Deloffre, J., Depreiter, D., Druine, F., Flöser, G., Grünler, S., Jourdin, F., Lafite, R., Nauw, J., Nechad, B., Röttgers, R., Sottolichio, A., Van Engeland, T., Vanhaverbeke, W., Vereecken, H., 2019. Uncertainties associated with in situ high-frequency long-term observations of suspended particulate matter concentration using optical and

acoustic sensors. Progress in Oceanography 178, 102162. https://doi.org/10.1016/j.pocean.2019.102162

Figueroa, S.M., Lee, G., Chang, J., Schieder, N.W., Kim, K., Kim, S.-Y., 2020. Evaluation of along-channel sediment flux gradients in an anthropocene estuary with an estuarine dam. Marine Geology 429, 106318. https://doi.org/10.1016/j.margeo.2020.106318

Fromant, G., Floc'h, F., Lebourges-Dhaussy, A., Jourdin, F., Perrot, Y., Le Dantec, N., Delacourt, C., 2017. In Situ Quantification of the Suspended Load of Estuarine Aggregates from Multifrequency Acoustic Inversions. Journal of Atmospheric and Oceanic Technology 34, 1625–1643. https://doi.org/10.1175/JTECH-D-16-0079.1

Geyer, W.R., MacCready, P., 2014. The Estuarine Circulation. Annu. Rev. Fluid Mech. 46, 175–197. https://doi.org/10.1146/annurev-fluid-010313-141302

Gong, W., Zhang, G., LirongYuan, Zhu, L., Zhang, H., 2022. Effects of swell waves on the dynamics of the estuarine turbidity maximum in an idealized convergent partially mixed estuary. Journal of Marine Systems 235, 103784. https://doi.org/10.1016/j.jmarsys.2022.103784

Grasso, F., Bismuth, E., Verney, R., 2021. Unraveling the impacts of meteorological and anthropogenic changes on sediment fluxes along an estuary-sea continuum. Scientific Reports 11, 20230. https://doi.org/10.1038/s41598-021-99502-7

Grasso, F., Le Hir, P., 2019. Influence of morphological changes on suspended sediment dynamics in a macrotidal estuary: diachronic analysis in the Seine Estuary (France) from 1960 to 2010. Ocean Dynamics 69, 83–100. https://doi.org/10.1007/s10236-018-1233-x

Grasso, F., Verney, R., Le Hir, P., Thouvenin, B., Schulz, E., Kervella, Y., Khojasteh Pour Fard, I., Lemoine, J.-P., Dumas, F., Garnier, V., 2018. Suspended Sediment Dynamics in the Macrotidal Seine Estuary (France): 1. Numerical Modeling of Turbidity Maximum Dynamics. Journal of Geophysical Research: Oceans 123, 558–577. https://doi.org/10.1002/2017JC013185

Halpern, B.S., Walbridge, S., Selkoe, K.A., Kappel, C.V., Micheli, F., D'Agrosa, C., Bruno, J.F., Casey, K.S., Ebert, C., Fox, H.E., Fujita, R., Heinemann, D., Lenihan, H.S., Madin, E.M.P., Perry, M.T., Selig, E.R., Spalding, M., Steneck, R., Watson, R., 2008. A Global Map of Human

Impact on Marine Ecosystems. Science 319, 948–952. https://doi.org/10.1126/science.1149345

Hesse, R.F., Zorndt, A., Fröhle, P., 2019. Modelling dynamics of the estuarine turbidity maximum and local net deposition. Ocean Dynamics 69, 489–507. https://doi.org/10.1007/s10236-019-01250-w

Jalón-Rojas, I., Schmidt, S., Sottolichio, A., 2015. Turbidity in the fluvial Gironde Estuary (southwest France) based on 10-year continuous monitoring: sensitivity to hydrological conditions. Hydrology and Earth System Sciences 19, 2805–2819. https://doi.org/10.5194/hess-19-2805-2015

Jalón-Rojas, I., Schmidt, S., Sottolichio, A., Bertier, C., 2016. Tracking the turbidity maximum zone in the Loire Estuary (France) based on a long-term, high-resolution and high-frequency monitoring network. Continental Shelf Research 117, 1–11. https://doi.org/10.1016/j.csr.2016.01.017

Jay, D.A., Talke, S.A., Hudson, A., Twardowski, M., 2015. Chapter 2 - Estuarine turbidity maxima revisited: Instrumental approaches, remote sensing, modeling studies, and new directions, in: Ashworth, P.J., Best, J.L., Parsons, D.R. (Eds.), Developments in Sedimentology. Elsevier, pp. 49–109. https://doi.org/10.1016/B978-0-444-63529-7.00004-3

Landemaine, V., 2016. Erosion des sols et transferts sédimentaires sur les bassins versants de l'Ouest du Bassin de Paris: analyse, quantification et modélisation à l'échelle plurianuelle (French version). Rouen University.

Le Hir, P., Ficht, A., Jacinto, R.S., Lesueur, P., Dupont, J.-P., Lafite, R., Brenon, I., Thouvenin, B., Cugier, P., 2001. Fine sediment transport and accumulations at the mouth of the Seine estuary (France). Estuaries 24, 950–963. https://doi.org/10.2307/1353009

Lemoine, J.P., Le Hir, P., 2021. Maintenance dredging in a macrotidal estuary: Modelling and assessment of its variability with hydro-meteorological forcing. Estuarine, Coastal and Shelf Science 258, 107366. https://doi.org/10.1016/j.ecss.2021.107366

Lesourd, S., Lesueur, P., Fisson, C., Dauvin, J.-C., 2016. Sediment evolution in the mouth of the Seine estuary (France): A long-term monitoring during the last 150years. Comptes Rendus Geoscience 348, 442–450. https://doi.org/10.1016/j.crte.2015.08.001

Leuven, J.R.F.W., Pierik, H.J., Vegt, M. van der, Bouma, T.J., Kleinhans, M.G., 2019. Sea-level-rise-induced threats depend on the size of tide-influenced estuaries worldwide. Nature Climate Change 9, 986–992. https://doi.org/10.1038/s41558-019-0608-4

Liu, G., Zhu, J., Wang, Y., Wu, H., Wu, J., 2011. Tripod measured residual currents and sediment flux: Impacts on the silting of the Deepwater Navigation Channel in the Changjiang Estuary. Estuarine, Coastal and Shelf Science 93, 192–201. https://doi.org/10.1016/j.ecss.2010.08.008

Liu, J., Li, Y., Pan, Q., Zhang, T., 2023. Suspended sediment transport and turbidity maximum in a macro-tidal estuary with mountain streams: A case study of the Oujiang Estuary. Continental Shelf Research 255, 104924. https://doi.org/10.1016/j.csr.2023.104924

Lotze, H.K., Lenihan, H.S., Bourque, B.J., Bradbury, R.H., Cooke, R.G., Kay, M.C., Kidwell, S.M., Kirby, M.X., Peterson, C.H., Jackson, J.B.C., 2006. Depletion, degradation, and recovery potential of estuaries and coastal seas. Science 312, 1806–1809. https://doi.org/10.1126/science.1128035

Manning, A.J., Bass, S.J., Dyer, K.R., 2006. Floc properties in the turbidity maximum of a mesotidal estuary during neap and spring tidal conditions. Marine Geology 235, 193–211. https://doi.org/10.1016/j.margeo.2006.10.014

McSweeney, J.M., Chant, R.J., Sommerfield, C.K., 2016. Lateral variability of sediment transport in the Delaware Estuary. Journal of Geophysical Research: Oceans 121, 725–744. https://doi.org/10.1002/2015JC010974

Mengual, B., Le Hir, P., Rivier, A., Caillaud, M., Grasso, F., 2021. Numerical modeling of bedload and suspended load contributions to morphological evolution of the Seine Estuary (France). International Journal of Sediment Research 36, 723–735. https://doi.org/10.1016/j.ijsrc.2020.07.003

Morelle, J., Schapira, M., Orvain, F., Riou, P., Lopez, P.J., Pierre-Duplessix, O., Rabiller, E., Maheux, F., Simon, B., Claquin, P., 2018. Annual Phytoplankton Primary Production Estimation in a

Temperate Estuary by Coupling PAM and Carbon Incorporation Methods. Estuaries and Coasts 41, 1337–1355. https://doi.org/10.1007/s12237-018-0369-8

Moskalski, S., Floc'h, F., Verney, R., 2020. Suspended sediment fluxes in a shallow macrotidal estuary. Marine Geology 419, 106050. https://doi.org/10.1016/j.margeo.2019.106050

Nicholls, R.J., Cazenave, A., 2010. Sea-Level Rise and Its Impact on Coastal Zones. Science 328, 1517–1520. https://doi.org/10.1126/science.1185782

Ody, A., Doxaran, D., Verney, R., Bourrin, F., Morin, G.P., Pairaud, I., Gangloff, A., 2022. Ocean Color Remote Sensing of Suspended Sediments along a Continuum from Rivers to River Plumes: Concentration, Transport, Fluxes and Dynamics. Remote Sensing 14. https://doi.org/10.3390/rs14092026

Pearson, S.G., Verney, R., van Prooijen, B.C., Tran, D., Hendriks, E.C.M., Jacquet, M., Wang, Z.B., 2021. Characterizing the Composition of Sand and Mud Suspensions in Coastal and Estuarine Environments Using Combined Optical and Acoustic Measurements. Journal of Geophysical Research: Oceans 126, e2021JC017354. https://doi.org/10.1029/2021JC017354

Phan, T.-T.-H., Poisson Caillault, É., Lefebvre, A., Bigand, A., 2020. Dynamic time warping-based imputation for univariate time series data. Pattern Recognition Letters 139, 139–147. https://doi.org/10.1016/j.patrec.2017.08.019

Poppeschi, C., Verney, R., Charria, G., submitted. Suspended particulate matter response to extreme forcings in the Bay of Seine. Submitted to Marine Geology.

Rodrigues, M., Cravo, A., Freire, P., Rosa, A., Santos, D., 2020. Temporal assessment of the water quality along an urban estuary (Tagus estuary, Portugal). Marine Chemistry 223, 103824. https://doi.org/10.1016/j.marchem.2020.103824

Roland, A., Ardhuin, F., 2014. On the developments of spectral wave models: numerics and parameterizations for the coastal ocean. Ocean Dynamics 64, 833–846. https://doi.org/10.1007/s10236-014-0711-z

Schettini, C.A.F., Duarte Pereira, M., Siegle, E., de Miranda, L.B., Silva, M.P., 2013. Residual fluxes of suspended sediment in a tidally dominated tropical estuary. Continental Shelf Research 70, 27–35. https://doi.org/10.1016/j.csr.2013.03.006

Schulz, E., Grasso, F., Le Hir, P., Verney, R., Thouvenin, B., 2018. Suspended Sediment Dynamics in the Macrotidal Seine Estuary (France): 2. Numerical Modeling of Sediment Fluxes and Budgets Under Typical Hydrological and Meteorological Conditions. Journal of Geophysical Research: Oceans 123, 578–600. https://doi.org/10.1002/2016JC012638

Sommerfield, C.K., Wong, K.-C., 2011. Mechanisms of sediment flux and turbidity maintenance in the Delaware Estuary. Journal of Geophysical Research: Oceans 116. https://doi.org/10.1029/2010JC006462

Sottolichio, A., Castaing, P., hetcheber, H., Maneux, E., Schmeltz, M., Schmidt, S., 2011. Observations of suspended sediment dynamics in a highly turbid macrotidal estuary, derived from continuous monitoring. Journal of Coastal Research 1579–1583.

Soulsby, R., 1997. Dynamics of marine sands. Thomas Telford Publishing. https://doi.org/10.1680/doms.25844

Stanton, T.K., Wiebe, P.H., Chu, D., 1998. Differences between sound scattering by weakly scattering spheres and finite-length cylinders with applications to sound scattering by zooplankton. The Journal of the Acoustical Society of America 103, 254–264. https://doi.org/10.1121/1.421135

Tavora, J., Boss, E., Doxaran, D., Hill, P., 2020. An Algorithm to Estimate Suspended Particulate Matter Concentrations and Associated Uncertainties from Remote Sensing Reflectance in Coastal Environments. Remote Sensing 12. https://doi.org/10.3390/rs12132172

Tessier, C., Le Hir, P., Lurton, X., Castaing, P., 2008. Estimation de la matière en suspension à partir de l'intensité rétrodiffusée des courantomètres acoustiques à effet Doppler (ADCP). Comptes Rendus Geoscience 340, 57–67. https://doi.org/10.1016/j.crte.2007.10.009

Thorne, P.D., MacDonald, I.T., Vincent, C.E., 2014. Modelling acoustic scattering by suspended flocculating sediments. Continental Shelf Research 88, 81–91. https://doi.org/10.1016/j.csr.2014.07.003

Uncles, R.J., Elliott, R.C.A., Weston, S.A., 1985. Observed fluxes of water, salt and suspended sediment in a partly mixed estuary. Estuarine, Coastal and Shelf Science 20, 147–167. https://doi.org/10.1016/0272-7714(85)90035-6

Verney, R., Deloffre, J., Brun-Cottan, J.-C., Lafite, R., 2007. The effect of wave-induced turbulence on intertidal mudflats: Impact of boat traffic and wind. Continental Shelf Research 27, 594–612. https://doi.org/10.1016/j.csr.2006.10.005

Verney Romaric, Le Berre David, Repecaud Michel (2024). COAST-HF - SCENES station dataset from 2015 to 2022 - environmental parameters. SEANOE. https://doi.org/10.17882/99434

Waeles, B., Le Hir, P., Lesueur, P., Delsinne, N., 2007. Modelling sand/mud transport and morphodynamics in the Seine river mouth (France): an attempt using a process-based approach. Hydrobiologia 588, 69–82. https://doi.org/10.1007/s10750-007-0653-2

Wang, Z.B., Elias, E.P.L., van der Spek, A.J.F., Lodder, Q.J., 2018. Sediment budget and morphological development of the Dutch Wadden Sea: impact of accelerated sea-level rise and subsidence until 2100. Netherlands Journal of Geosciences 97, 183–214. https://doi.org/10.1017/njg.2018.8

Wetsteyn, L.P.M.J., Kromkamp, J.C., 1994. Turbidity, nutrients and phytoplankton primary production in the Oosterschelde (The Netherlands) before, during and after a large-scale coastal engineering project (1980–1990), in: Nienhuis, P.H., Smaal, A.C. (Eds.), The Oosterschelde Estuary (The Netherlands): A Case-Study of a Changing Ecosystem. Springer Netherlands, Dordrecht, pp. 61–78. https://doi.org/10.1007/978-94-011-1174-4_7

Worm, B., Barbier, E.B., Beaumont, N., Duffy, J.E., Folke, C., Halpern, B.S., Jackson, J.B.C., Lotze, H.K., Micheli, F., Palumbi, S.R., Sala, E., Selkoe, K.A., Stachowicz, J.J., Watson, R., 2006. Impacts of Biodiversity Loss on Ocean Ecosystem Services. Science 314, 787–790. https://doi.org/10.1126/science.1132294

10. Appendices

10.1. *Evaluating bottom SPMC from ADP backscatter data*

The Sonar equation is used to convert the raw acoustic backscatter into decibels and correct it for geometric and near-field corrections, spherical spreading and water attenuation, as detailed in Fettweis et al. (2019) and Tessier et al. (2008). As SPMC can be temporary higher than 0.1g/l close to the bed (i.e. below 1.5m), sediment attenuation is also taken into account, using an iterative method as described in Thorne et al. (2014). From the Sonar equation, a backscatter index (BI) is calculated such as:

$$N + K_c\,(E - E_0) = SL - 20\,log_{10}(\psi R^2) - 2\int_0^R (\alpha_w(r) + \alpha_s(r))dr$$

$$+BI + 10log_{10}\left(\varphi R^2 \frac{WS}{2}\right) \quad \text{(Eq. 3)}$$

Where E is the echo amplitude recorded by the ADP, N and E_0 the noise and reference acoustic level, Kc the conversion constant from count to dB, SL the source level (dB), R the distance from transducer to cell, y the near-field correction factor, a_w and a_s the water and sediment attenuation respectively, WS the cell size, j the solid angle and BI the backscatter index.

The raw echo amplitude signal E recorded by the ADP can be significantly lowered due to biofouling as well as decreasing battery level. During the first weeks of the deployment of brand-new ADP, the amplitude signal recorded for low turbidity values (between 2 to 5NTU) is measured on average around 150count. As a first step, an offset per tide is calculated such as the raw echo amplitude signal in count is 150count for turbidity values at 1.4mab ranging from 2 to 5NTU. However, this correction is not applicable to long periods when turbidity remains high above 5NTU over the tidal cycle, as observed during winter time. When applicable, the correction value is then interpolated.

BI is directly related to SPM characteristics (e.g. median diameter, D50), using acoustic/floc hybrid interaction model developed by Thorne et al. (2014):

$$\boldsymbol{BI = 10log_{10}\left(\frac{SSC\,\bar{\sigma}}{\rho_s\,\overline{v_s}}\right) = 10log_{10}(SSC) + f\left(D50_{opt-acc}\right)} \qquad \text{(Eq. 4)}$$

With s the backscattering cross section, r_s and v_s the representative floc volume and density (Stanton et al., 1998; Thorne et al., 2014 – n_f=2; D_p=4mm). At this stage, this optimal $D50_{opt\text{-}acc}$ must be considered as an equivalent acoustic calibration parameter, and not necessary as an absolute physical characteristic of SPM.

The temperature is recorded close to the bed and considered constant over the water column. The salinity is not necessarily known, and first considered constant, at 34PSU.

In this section we only consider the acoustic backscatter at the first cell of the ADP, and calibrate it against the SPMC recorded 1.4mab, i.e. at the elevation of the first bin of the ADP. $D50_{opt\text{-}acc}$ is calculated to retrieve the optical-derived SPMC, outside the saturation regime. $D50_{opt\text{-}acc}$ strongly varies at the tidal scale and also fortnightly. In order to evaluate an appropriate $D50_{opt\text{-}acc}$ within the saturation regime, the $D50_{opt\text{-}acc}$ time series is tide-separated, from low tide to the following low tide, and classified by tidal range and wave conditions. The intratidal time series for a given tidal range are then averaged to produce a climatology for $D50_{opt\text{-}acc}$ (refer to section 3.5.5. for method). This $D50_{opt\text{-}acc}$ climatology (Figure 17) is used to estimate bottom SPMC when the optical sensor reaches the saturation regime.

From November 2021 and March 2022, a high-range (0-1000NTU) optical Wetlabs FLNTU turbidity meter was deployed, hence significantly limiting saturation. This period is used to evaluate our capacity to compensate for saturated data using acoustic measurements.

Applying $D50_{opt\text{-}acc}$ to evaluate saturated SPMC provides reasonable but still uncertain quantification of D50 and hence SPMC (Figure 18 left). This is probably due to incomplete correction of the biofouling effect by correcting the raw echo amplitude. The next step in postprocessing (detailed below) can be separated in two situations, depending if turbidity is fully or partly saturated over the tidal cycle. For each situation, the $D50_{opt\text{-}acc}$ tidal climatology is modulated by multiplying $D50_{opt\text{-}acc}$ with a correction factor k_{opt} ranging from 0 to 2.

If turbidity data are fully saturated over the whole tidal cycle, the optimal correction factor k_{opt} corresponds to calculated tidal acoustic SPMC with all N values per tide above the saturation concentration (0.085g/l) and the closer to 1, meaning the lowest compensation is applied.

$$\begin{cases} \sum_{1}^{N} \left(SSC_{opt-acc}(k_{opt}) > SSC_{saturation}\right) = N \\ \quad \& \\ abs(k_{opt} - 1) = \min(abs(k-1)) \end{cases}$$

(Eq. 5)

If saturation is partial and only concern N_{sat} (N_{sat}<N) values per tidal cycle, the optimal correction factor k_{opt} is calculated from a cost function based on the combination of calculated acoustic SPMC values above the saturation concentration when saturated and a good fit with observed non saturated data:

$$\begin{cases} fac_{sat}(k) = \frac{1}{N_{sat}} \sum_{1}^{N_{sat}} \left(SSC_{opt-acc}(k) > SSC_{saturation}\right) \\ fac_{obs}(k) = abs\left(\langle \frac{(SSC_{opt-acc}(k) - SSC_{obs}}{SSC_{obs}} \rangle\right) \\ fac(k) = \min\left(fac_{obs}(k) * \left(1 - \frac{N_{sat}}{N}\right) + fac_{sat}(k) * \frac{N_{sat}}{N}\right) \\ fac\left(k_{opt}\right) = \min\left(fac(k)\right) \end{cases}$$

(Eq. 6)

Figure 18 illustrates the efficiency of the saturation compensation method from acoustic inversion using high-range turbidity measurements. Adapting climatology provides better SPMC estimation for low concentration values (0-0.1g/l), but also and more important in high SPMC ranges (>0.1g/l). While median acoustic SPMC values reach a threshold around the saturation value when using raw climatology, the compensation method provides far better SPMC estimation, while still underestimating SPMC for values above 0.1g/l. The latter can be explained by the absence of reference data available to contribute to scale the correction factor when all the tidal cycle is saturated. In such situation k_{opt} is chosen to compute SPMC just above the saturation concentration, but during intense energetic events (i.e. large resuspension events), the "real" concentration can be significantly larger.

10.2. Evaluating depth-varying SPM concentration from ADP measurements

ADP measurements are largely used to evaluate SPMC in the water column. Similarly to bottom SPMC, this requires to correctly calibrate the optimal D50 in each cell, without additional observation other than bottom and surface optical SPMC. This section details the method applied to retrieve SPMC concentration over the whole water column and for all acoustic profile over the 7year period.

Based on ship-based surveys and vertical SPMC profiles at the tidal cycle, it is possible to calculate this parameter for the 19 tidal cycles. The optimal D50 for each bin is estimated using the Sonar equation to match the observed optical SPMC in the water column, as illustrated in Figure 19. The D50 vertical dynamics significantly changes at tidal scale: strong vertical D50 gradients are observed, during flood and ebb phases, at different relative depth, e.g. decreasing from ~110µm close to the bed to ~50µm in the top half of the water column in 2015. We can also note that the dynamics is different before and after October 2017, associated with a change in bottom deployments: while D50 generally decreases from bottom to surface before October 2017 (i.e. 2015) during flood phase, D50 is maximum in the middle of the water column after October 2017. This is possibly due to the extrapolation of the SPMC 1.4mab during the second phase, which contains uncertainties. This can

imply larger $D50_{opt\text{-}acc}$, which are used to normalize the D50 vertical profile. Two different D50 extrapolation methods are then searched to estimate the vertical distribution of D50 for each period.

All ship-based tidal cycles available for each period are used and cast time recalculated with the local low-tide time as reference. Vertical bin depths are normalized with the corresponding water depth, hence varying from 0 (bottom) to 1 (surface). For each cast, D50(z) are normalized by the bottom $D50_{opt\text{-}acc}$ estimated from bottom SPMC. Finally, all normalized D50 casts for all tidal cycles per period are grouped hourly from low tide, and averaged to provide hourly mean normalized D50 vertical profile at the tidal scale (Figure 20) and noted $D50_{z\_norm}$. As subsurface acoustic data often interfere with sea surface and wave-generated bubbles, $D50_{z\_norm}$ values are frozen to the value calculated at 80% of the total depth, corresponding to the depth of the sub-surface optical turbidity sensor. Before October 2017, $D50_{z\_norm}$ decreases from bottom to surface by 20% to 40% compared to bottom $D50_{opt\text{-}acc}$. During the second period (after October 2017), $D50_{z\_norm}$ first increases by 20 to 30% in the bottom third of the water column and decreases above, except around low tide.

This method ensures that the calculated bottom SPM concentrations using the acoustic backscatter signal still compare exactly with the bottom $SPMC_{opt\text{-}acc}$ at all times. A last correction must be included to ensure that surface SPMC from the acoustic signal also compare with the surface SPMC derived from the optical turbidity sensors. Similarly to bottom SPMC, two equivalent D50 are calculated based on observed surface SPMC 1.5m (optical sensor level) and 2.5m below surface. Two D50 are calculated as the acoustic backscatter can be impacted by air bubbles generated by waves or by sea surface reflection, and the $D50_{1.5bs}$ calculated 1.5m below surface can be biased. A $D50_{2.5bs}$ (2.5m below surface) is also calculated from the observed surface SPMC, assuming low subsurface SPMC gradients.

Next, a vertical surface correction (cor_{surf_z}) is computed. Below mid-depth, cor_{surf_z} equals 1, and no correction is applied. At 80% of the water depth, the $D50_{2.5m}$ is forced to coincide with the optimal

D50, and at 85% of the water column and higher, $D50_{1.5bs}$ is forced. From mid depth to 80% of the total depth, a linear interpolation is applied such as:

$$\begin{cases} \mathrm{cor}_{\mathrm{surf_z}}\left(\frac{z}{h}\right) = 1 \ \text{ if } \ \frac{\mathrm{z}}{\mathrm{h}} \leq 0.5 \\ \mathrm{cor}_{\mathrm{surf\_z}}\left(\frac{z}{h}\right) = \mathrm{linear\_interp}\left(\left[\mathrm{cor}_{\mathrm{surf\_z}}\left(\frac{z}{h}=0.5\right)\ ;\ \mathrm{cor}_{\mathrm{surf\_z}}\left(\frac{z}{h}=0.8\right)\right], \frac{z}{h}\right) \ \text{ if } \ 0.5 < \frac{\mathrm{z}}{\mathrm{h}} < 0.80 \\ \mathrm{cor}_{\mathrm{surf\_z}}\left(\frac{z}{h}\right) = \frac{\mathrm{D50}_{2.5\mathrm{bs}}}{D50_{opt-acc} * D50_{z\_norm}\left(\frac{z}{h}\right)} \ \ if \ \frac{z}{h} = 0.8 \\ \mathrm{cor}_{\mathrm{surf\_z}}\left(\frac{z}{h}\right) = \frac{\mathrm{D50}_{1.5\mathrm{bs}}}{D50_{opt-acc} * D50_{z\_norm}\left(\frac{z}{h}\right)} \ \ if \ \frac{z}{h} \geq 0.85 \end{cases}$$

(Eq. 7)

Finally, the vertical D50 array at each time is calculated such as:

$$D50\left(\frac{z}{h}\right) = \mathrm{cor}_{\mathrm{surf\_z}}\left(\frac{z}{h}\right) * D50_{opt-acc} * D50_{z\_norm}\left(\frac{z}{h}\right)$$

(Eq. 8)

Using Eq. 3 and Eq. 4 solving the Sonar equation, the SPM concentration at all times and all bins in the water column can be computed from ADP backscatter data and compared with ship-based SPMC measurements.

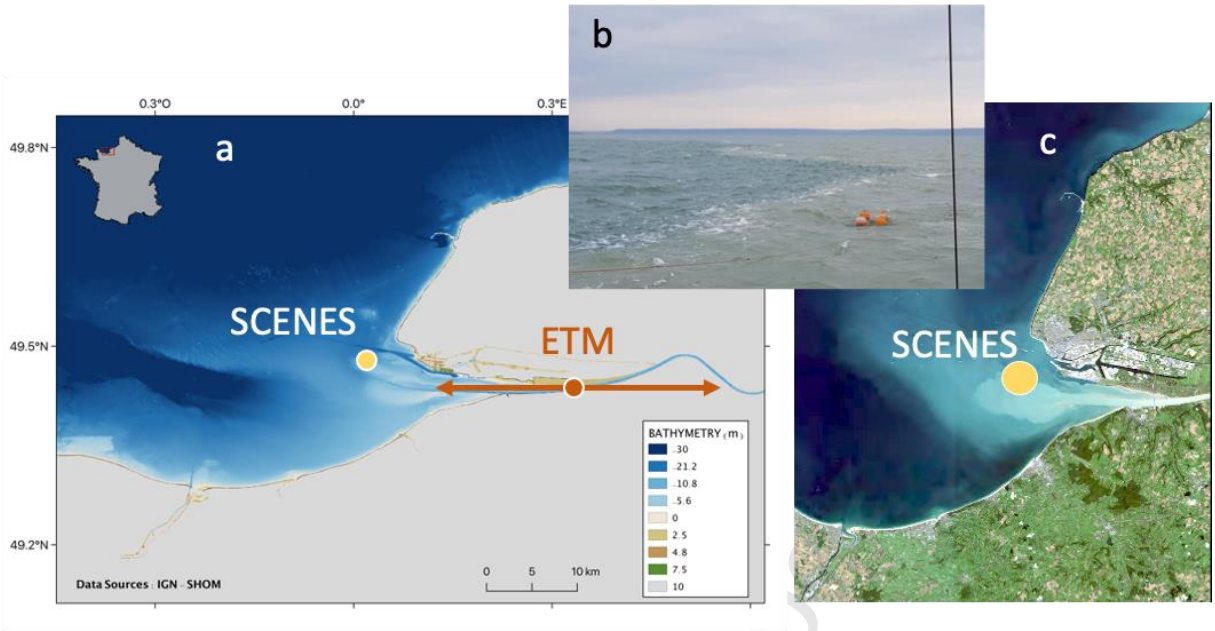

Figure 1: Seine estuary and bay: bathymetry and location of the SCENES station (a), picture of the frontal structure of the turbid plume at SCENES (b) and Landsat 8 images of surface turbidity plume(c).

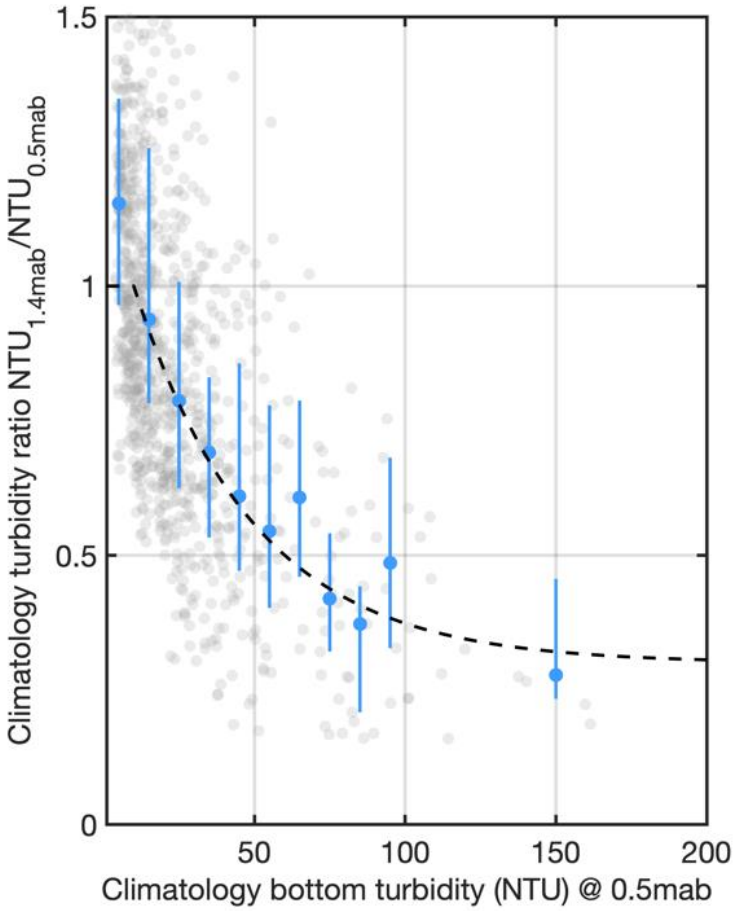

Figure 2: Evolution of intratidal turbidity climatology ratio between 2015-2017/06 (measured at 1.4mab) and 2017/10-2022 (measured at 0.5mab) as a function of turbidity at 0.5mab. Raw data are marked by grey dots, blue dots represent median values per turbidity classes and vertical bars the percentiles 25 and 75.

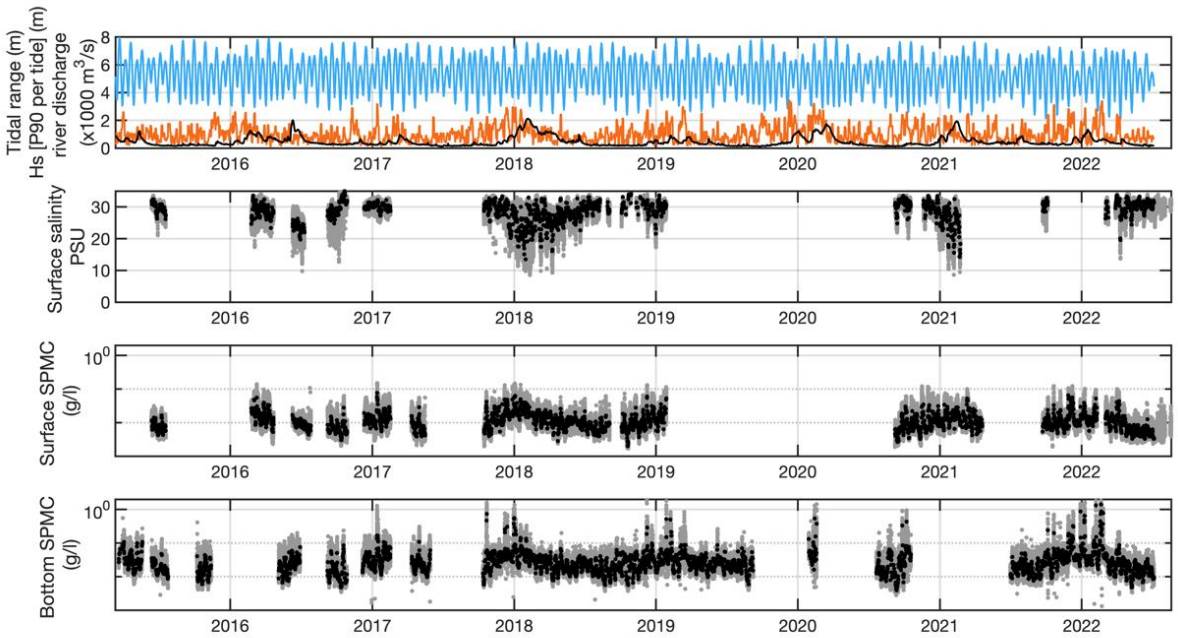

Figure 3: Hydro-meteorological and tidal forcing and SPM concentration dynamics from 2015 to 2022 at the mouth of the Seine Estuary. Top: River discharge (black), tidal range (blue) and waves (Hs_{P90} - red); middle: surface SPMC; bottom: bottom SPMC. (grey dots: raw high-frequency concentration; black dots: tidal-median SPMC). Time labels indicate the first day of each year.

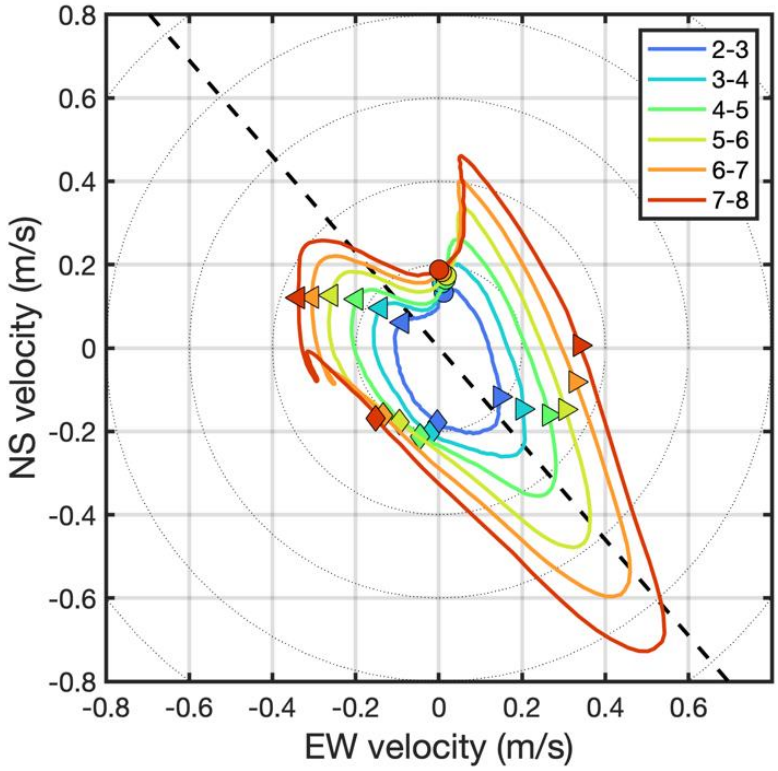

Figure 4: Average barotropic current velocity ellipses per tidal range classes (line colour) (Eastward and Northward positive). Diamonds represent low tide, circles high tide, right and left triangles +3h and -3h after low tide respectively. Grey circles represent velocity magnitude. Dashed line indicates the current direction during flood.

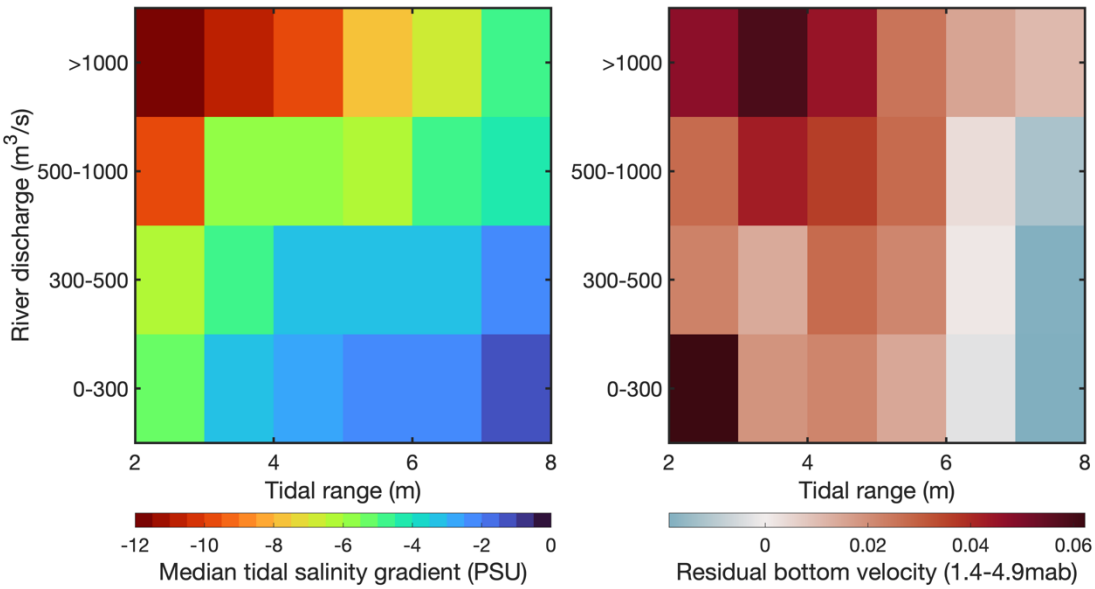

Figure 5: Tidal median vertical salinity gradient (Surface-Bottom) (left) and residual bottom (1.4-4.9m above bed) velocities (right) as a function of river discharge and tidal range classes, for low wave conditions (Hs_{P90}<1m)

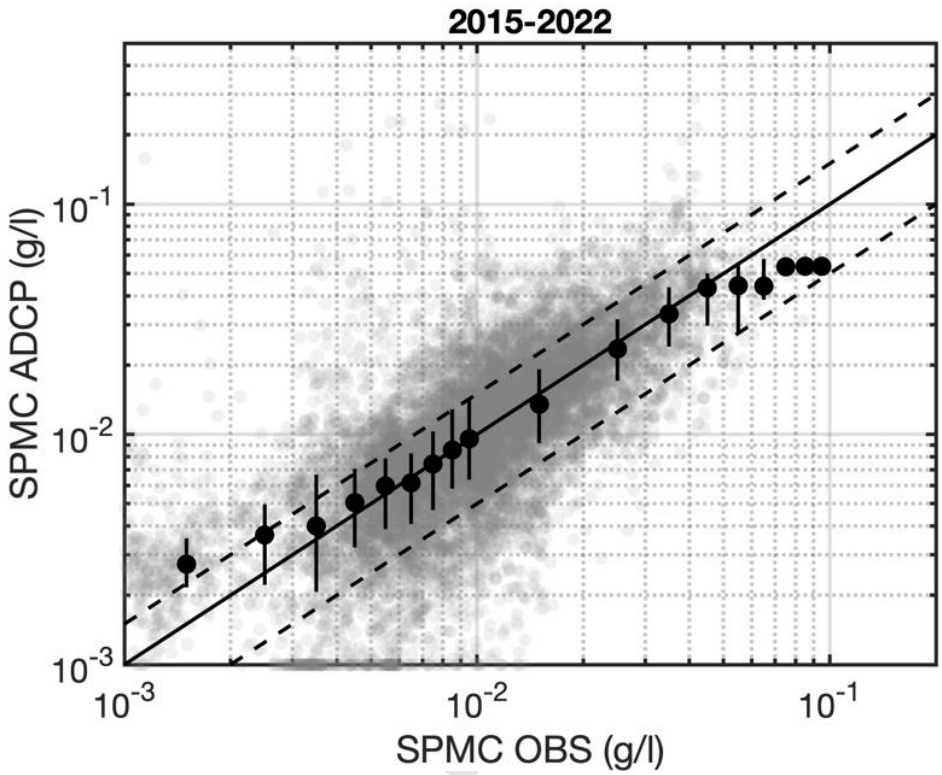

Figure 6: Comparison between ship-based SCC cast data and ADP SPMC data for 19 tidal cycles from 2015 to 2022. Grey points show raw data, black points the median per SPMC classes (every 0.01g/l below 0.1g/l; every 0.1g/l above 0.1g/l). Vertical bars show percentiles 25 and 75 per SPMC class. Black line is the 1:1 line, and the dashed lines represent +/-50% interval

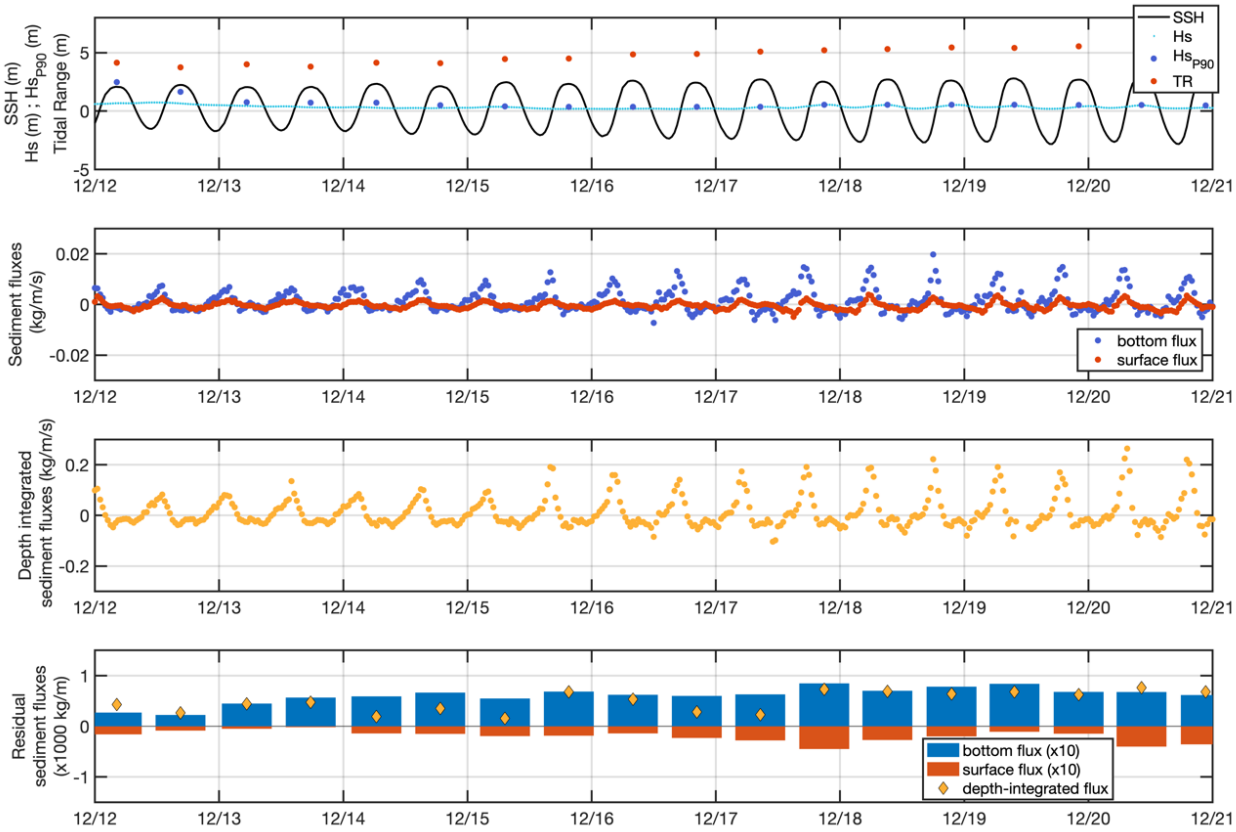

Figure 7: Tidal range, sea surface height, significant wave height (raw and tidal P90) (a) and SPM fluxes during calm weather conditions (Hs_{P90}<1m) (12/12/2021-20/12/2021): Surface and bottom fluxes (b); depth-integrated fluxes (c) and residual (surface, bottom and depth-integrated) fluxes (d).

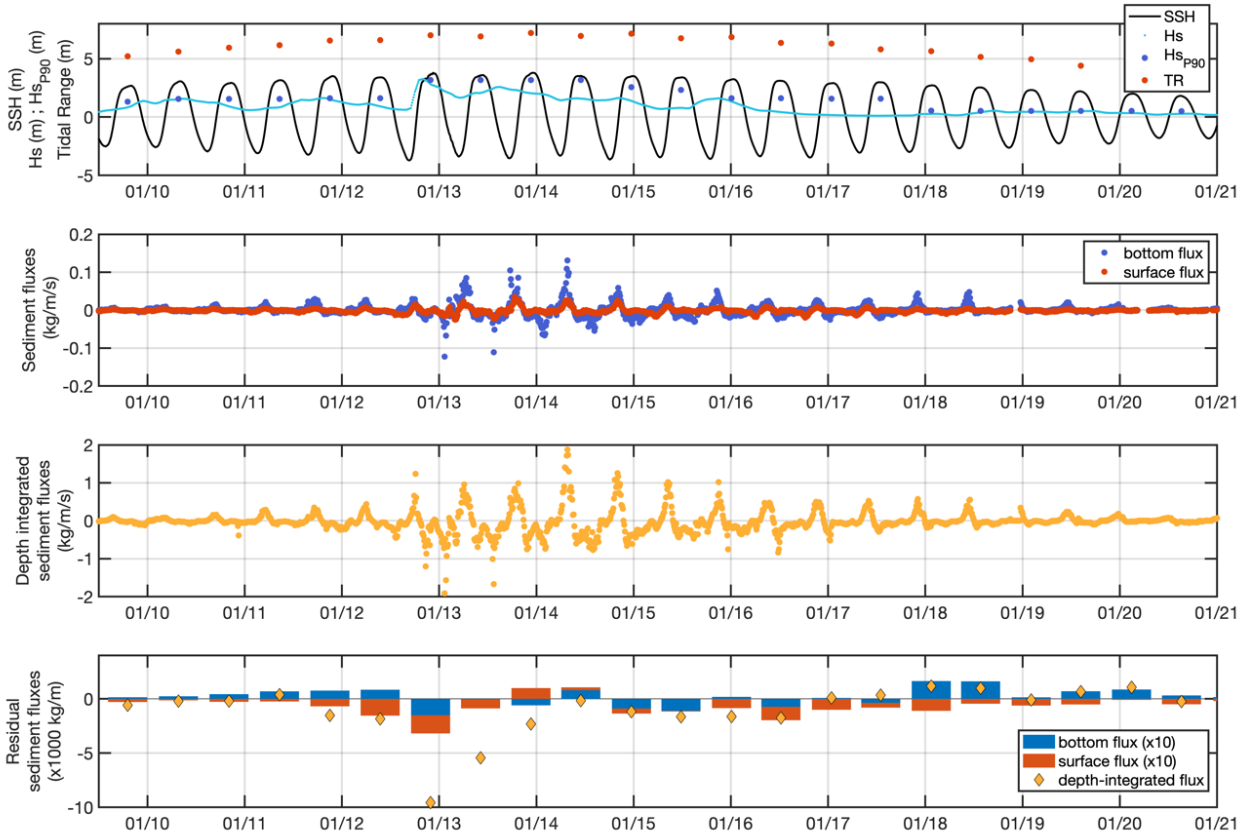

Figure 8: Tidal range, sea surface height, significant wave height (raw and tidal P90) (a) and SPM fluxes during stormy conditions (Hs_{P90}>2m) (9/1/2017-21/1/2017): Surface and bottom fluxes (b); depth-integrated fluxes (c) and residual (surface, bottom and depth-integrated) fluxes (d).

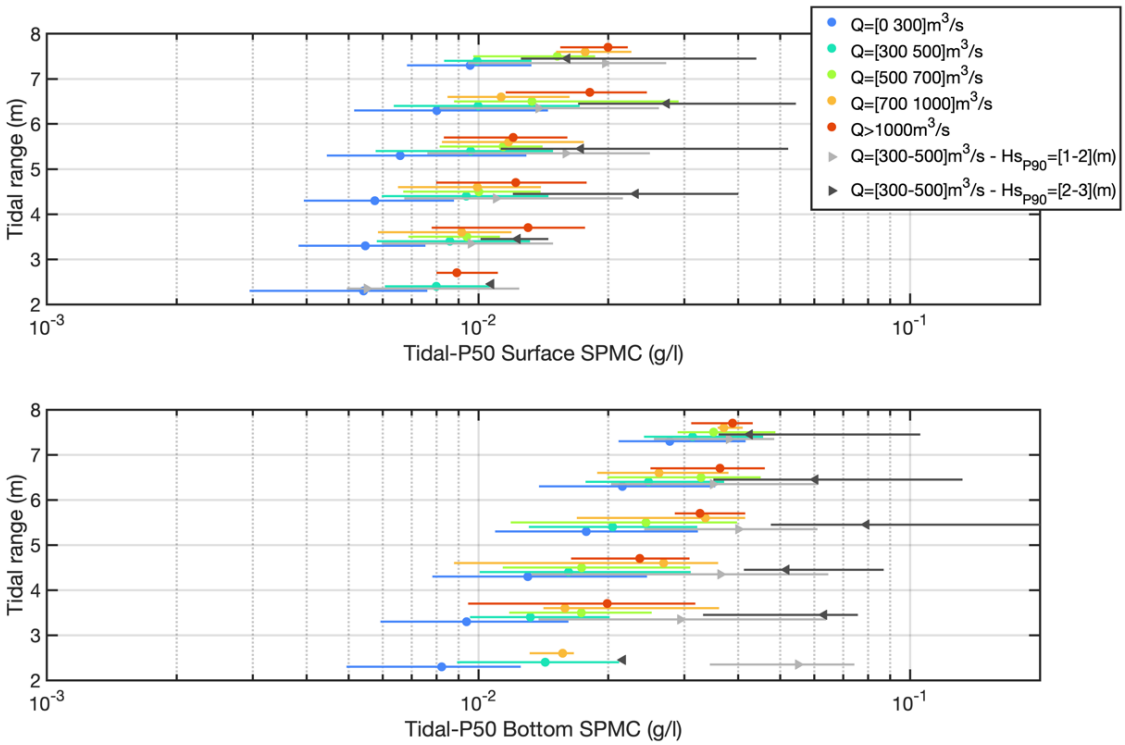

Figure 9: Variability of the tidal-median SPMC concentration at surface (top) and bottom (bottom) for different conditions of tidal range, river discharge (colour), and Hs_{P90} (triangles). Markers represent the median value per condition, and lines the extension between the percentile 10 and 90. Wave conditions are only shown for river discharge conditions from 300m^3/s to 500m^3/s.

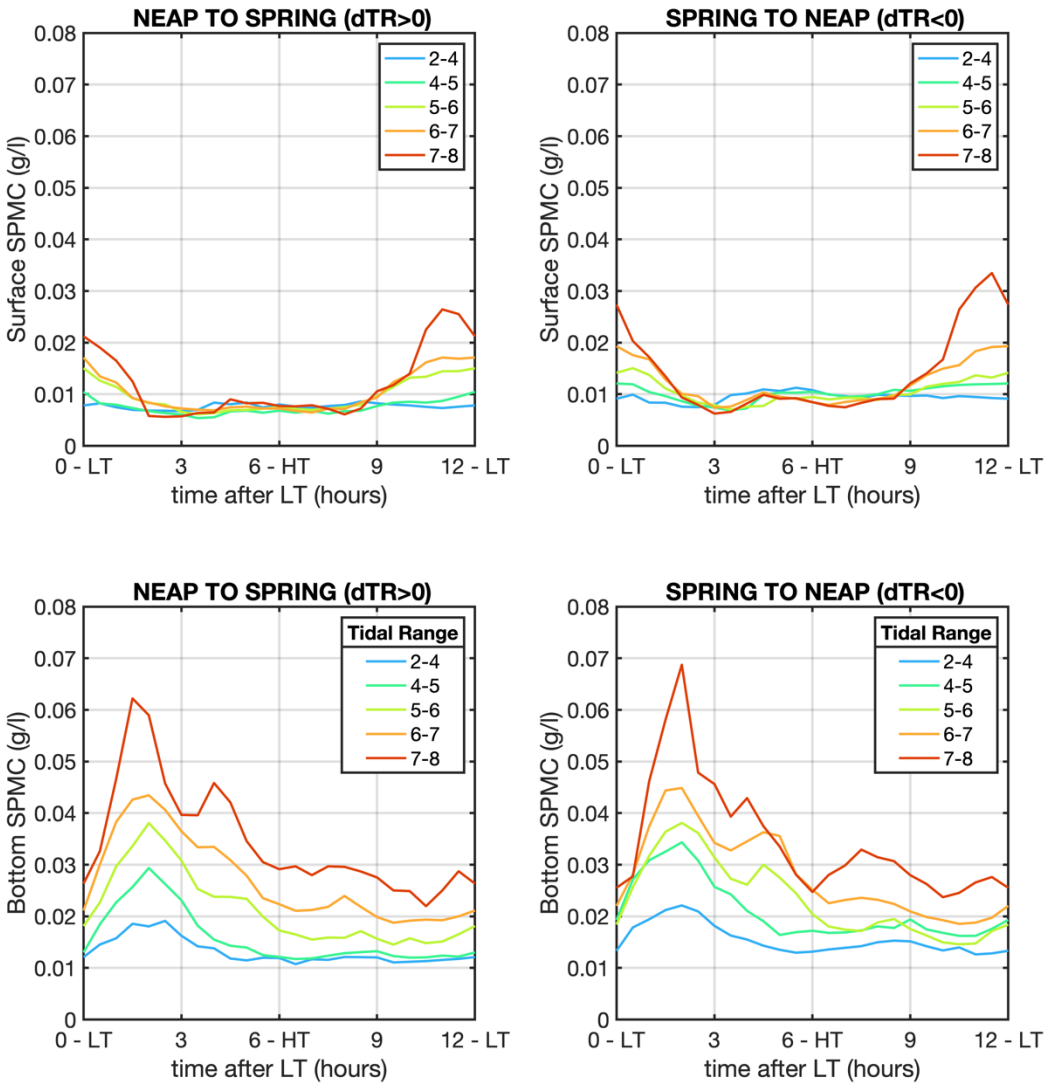

Figure 10: Intratidal SPMC climatology for different conditions of tidal range and tidal range gradients. Climatologies are computed for low wave conditions (Hs_{P90}<1m) and average river discharge conditions ([300-500]m^3/s). Top: surface intratidal SPMC; Bottom: bottom intratidal SPMC; Left: positive tidal range gradients (from neap to spring); Right: negative tidal range gradients (from spring to neap).

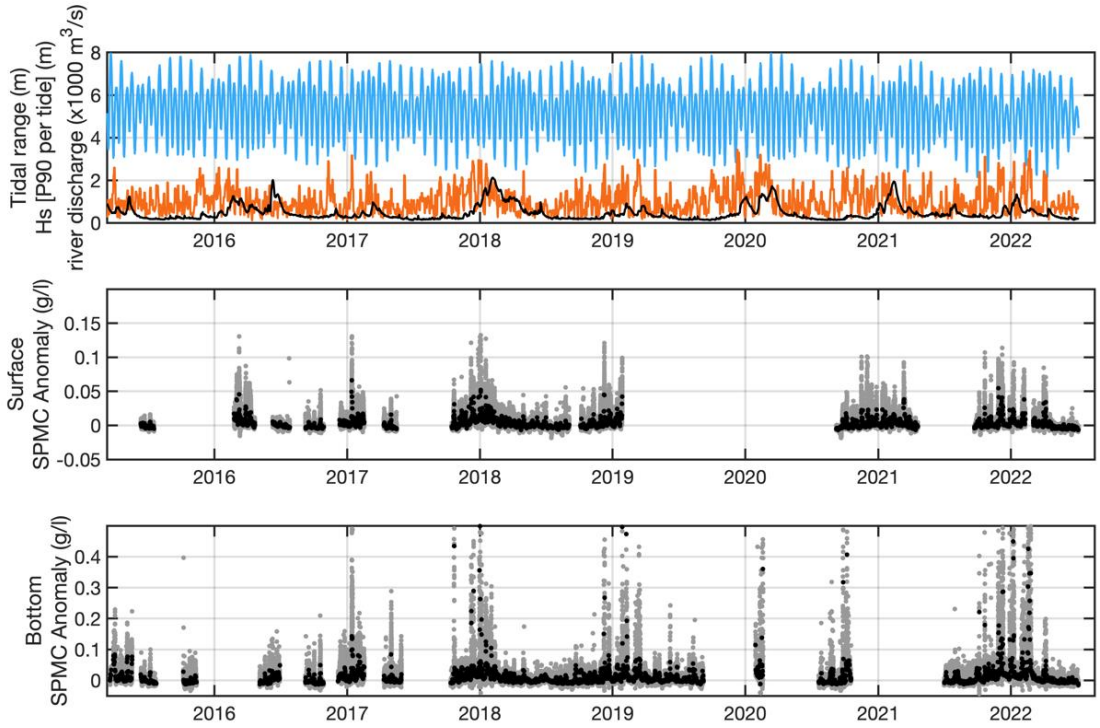

Figure 11: Hydro-meteorological and tidal forcing and SPM concentration anomalies from 2015 to 2022 at the mouth of the Seine Estuary. X-labels indicate the first day of each year . Top: River discharge (black line), tidal range (blue line) and waves (HsP90) (orange line); Middle: surface SPMC anomaly; Bottom: bottom SPMC anomaly (grey dots: raw high-frequency SPMC anomaly; black dots: tidal-median SPMC anomaly).

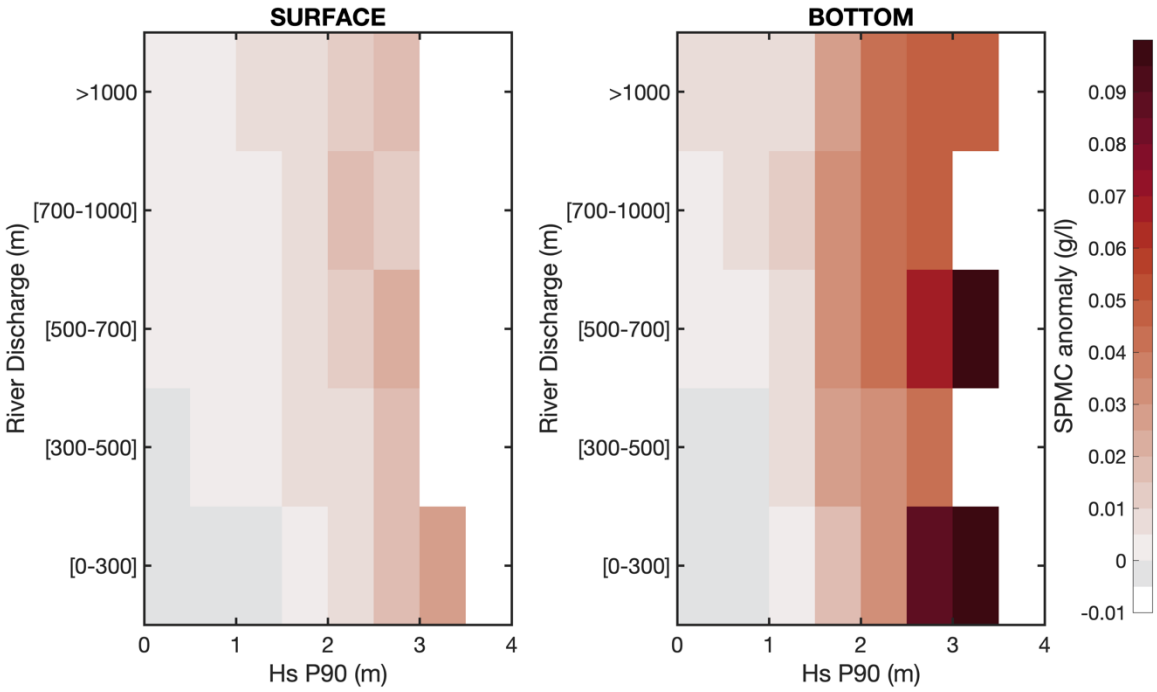

Figure 12: Tidal-median SPMC anomaly as a function of river discharge and wave (Hs_{P90}) conditions. Left: surface; Right: bottom.

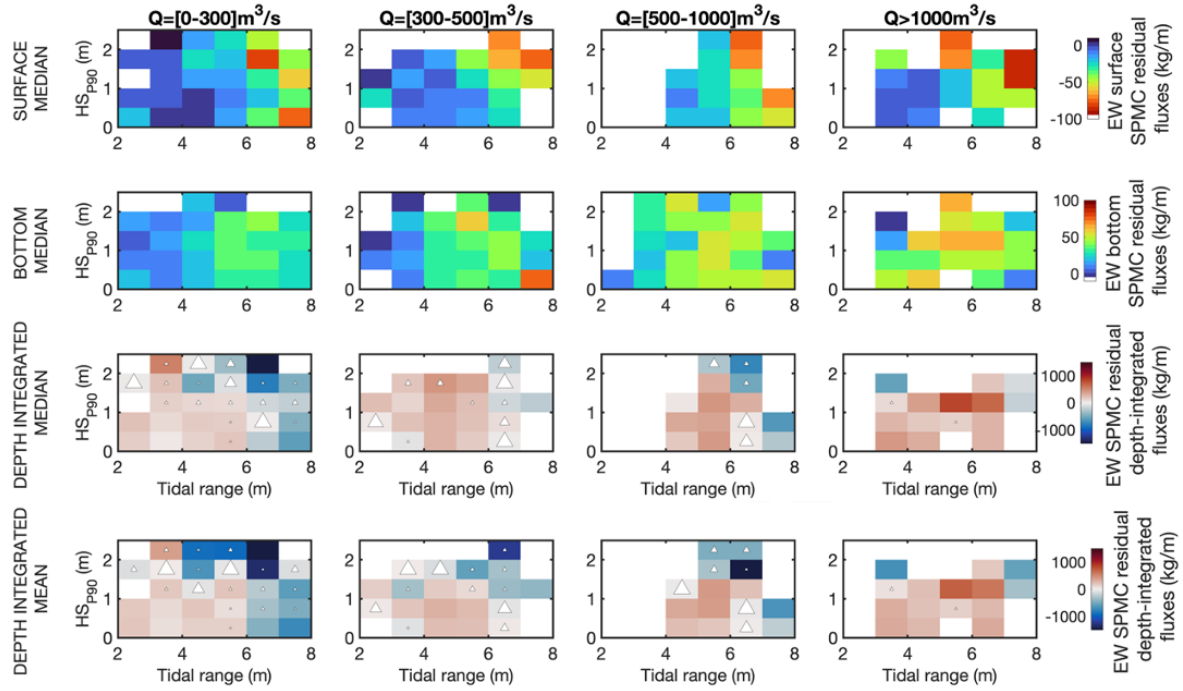

Figure 13: Median (row 1-3) and mean (row 4) residual fluxes per wave, tidal range and river discharge conditions. Different fluxes are evaluated: Surface, bottom and depth-integrated fluxes (at least 5 tides per hydro-meteorological conditions). White triangles represent the uncertainty U_F of the median depth-integrated residual fluxes (percentile 25 or 75 with an opposite sign as the median). The triangle size indicates uncertainty intensity.

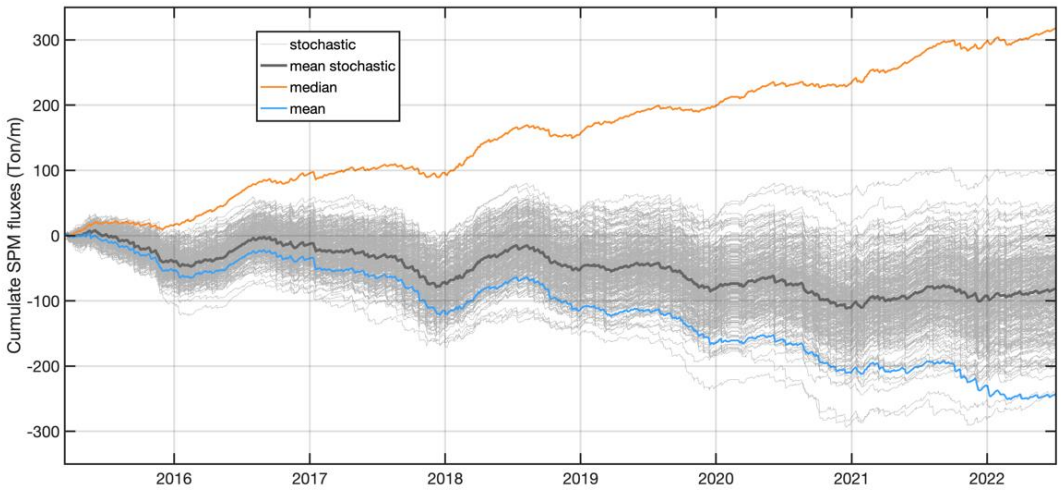

Figure 14: SPM cumulative residual fluxes over the period 2015-2022. Thin grey lines represent fluxes estimated from stochastic analysis using the residual flux probability density function for each river discharge, wave and tidal condition. Thick dark grey line shows the mean of the stochastic fluxes. Blue and orange lines represent cumulative fluxes using mean and median residual flux calculation per conditions.

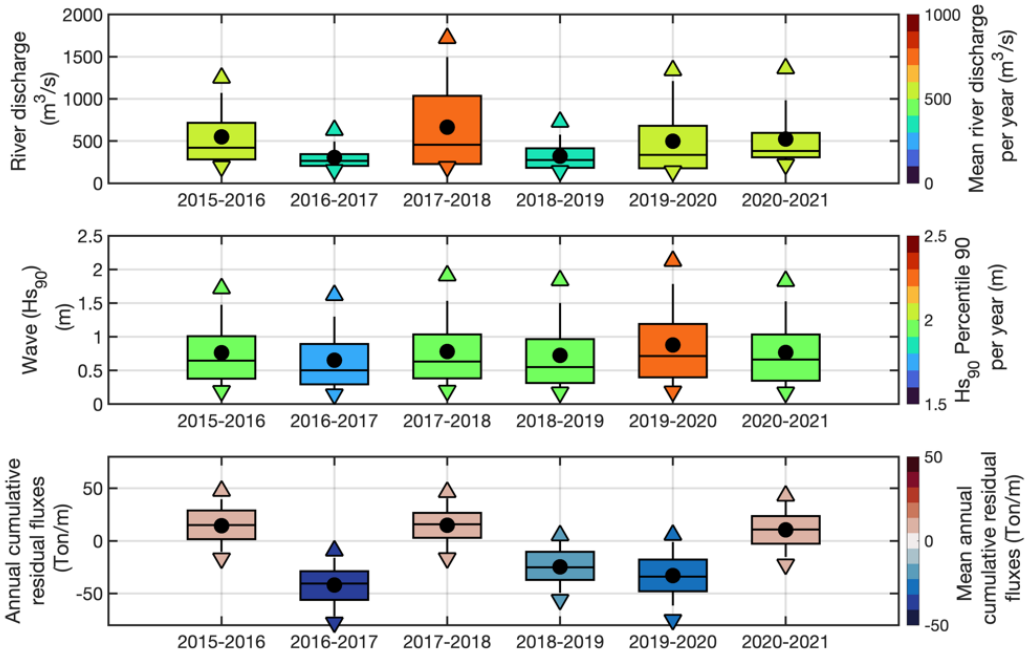

Figure 15: Annual statistics of river discharge (top), tidal percentile 90 of significant wave height (middle) and cumulative residual fluxes (bottom) from 2015 to 2021. Hydrological years are considered to separate annual time series, i.e. from October to October.

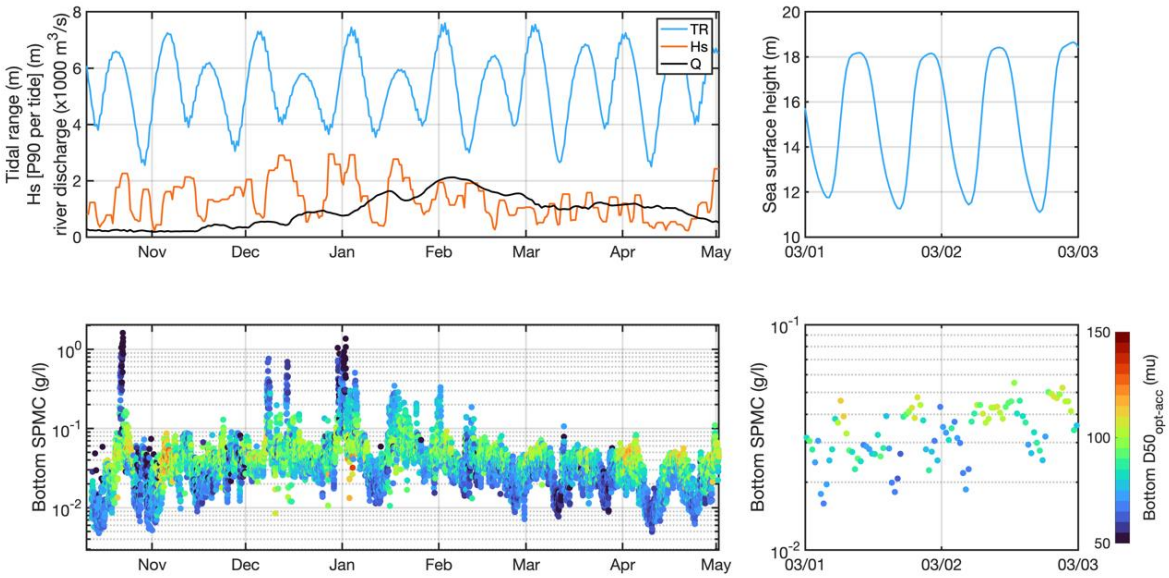

Figure 16: Hydro-meteorological and tidal forcing and bottom SPM concentration from October 2017 to may 2018 at the mouth of the Seine Estuary. Top left: River discharge, tidal range and waves (HsP90); Bottom left: bottom SPMC and $D50_{opt-acc}$ (colour); Top right: water level – focus from march 1st to march 3rd, 2018 (red rectangle); Bottom right: bottom SPMC and $D50_{opt-acc}$ (colour)

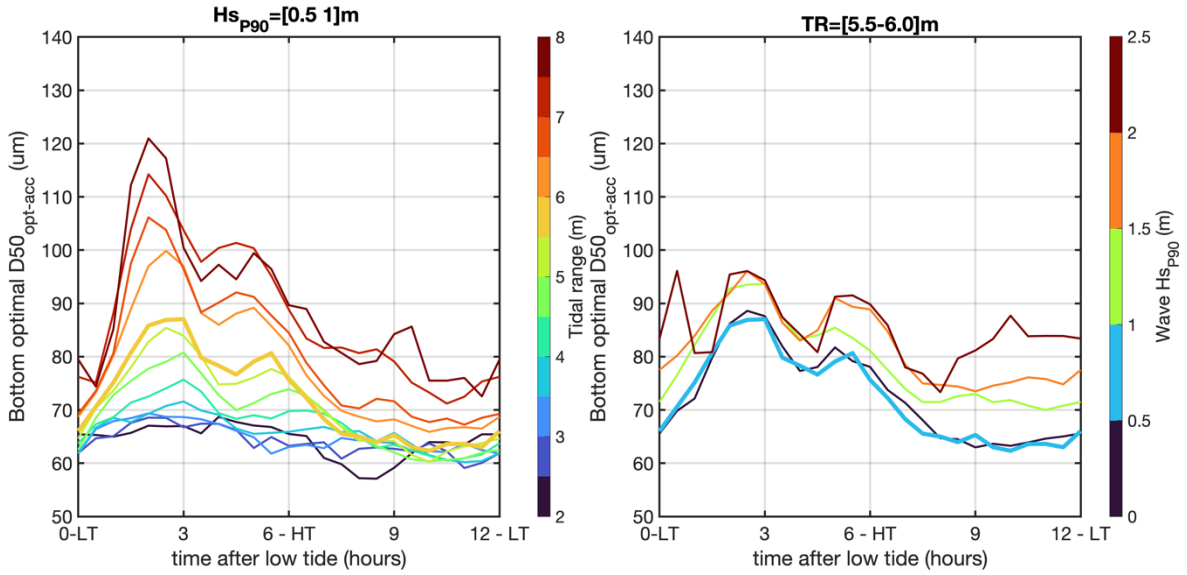

Figure 17: Intratidal D50$_{opt-acc}$ climatology calculated over the period 2015-2022. Left: intratidal D50$_{opt-acc}$ over tidal range (for low wave activity: Hs$_{P90}$=[0.5-1]m). Right: intratidal D50opt-acc over wave Hs$_{P90}$ range (for TR=[5.5-6]m)

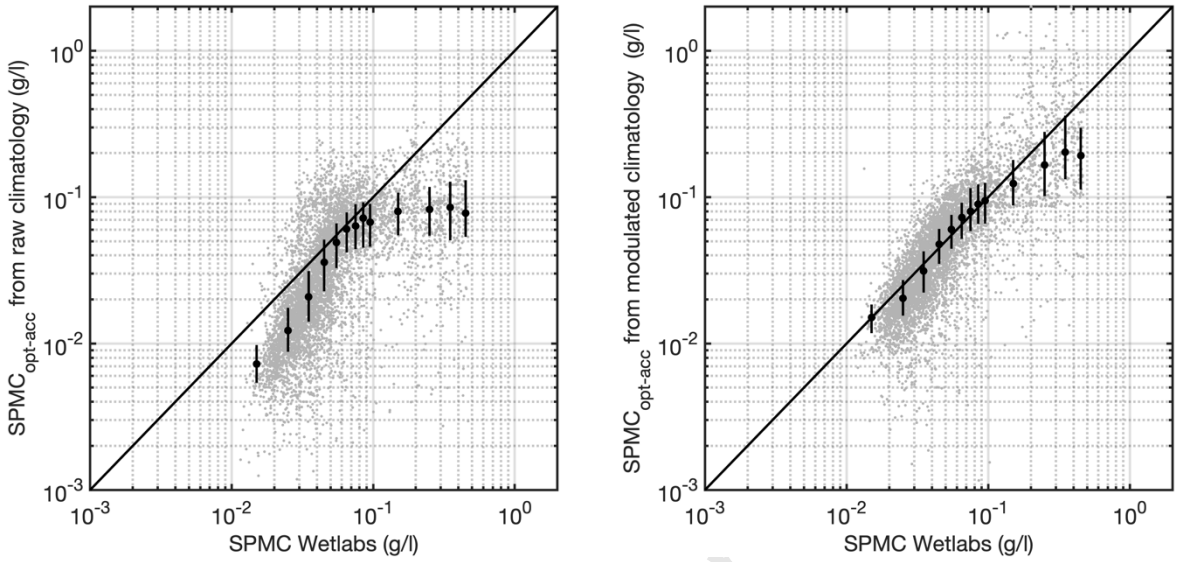

Figure 18: Comparison of non-saturated observed SPMC data (from November 2021 to March 2022) with SPMC calculated from acoustic inversion, using the raw $D50_{opt\text{-}acc}$ climatology (left) and the modulated $D50_{opt\text{-}acc}$ climatology (right). Gray dots show raw data, black dots median $SPMC_{opt\text{-}acc}$ data per SPMC Wetlabs classes, and vertical bars show percentile 25 and 75 values.

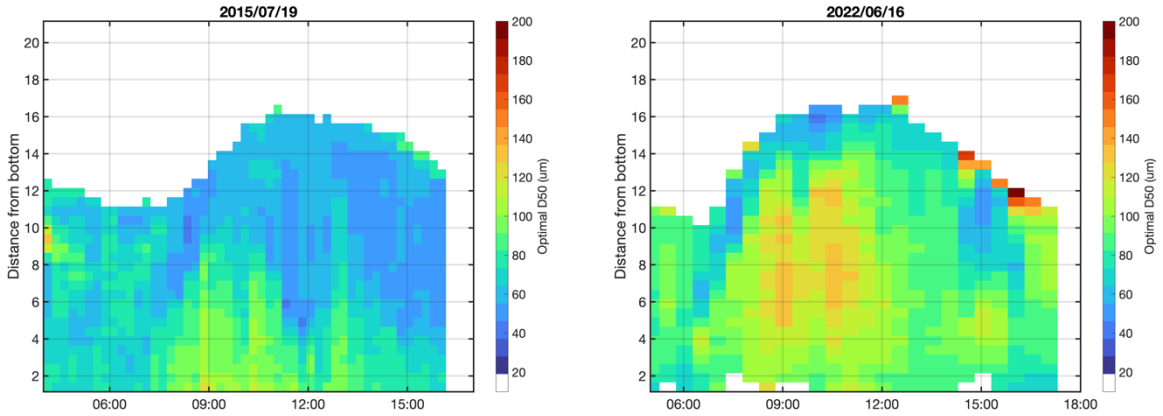

Figure 19: Optimal acoustic D50 from the inversion of the acoustic backscatter signal and ship-based SPMC profiles during two tidal cycles (left: 19th July 2015; right: 16th June 2022).

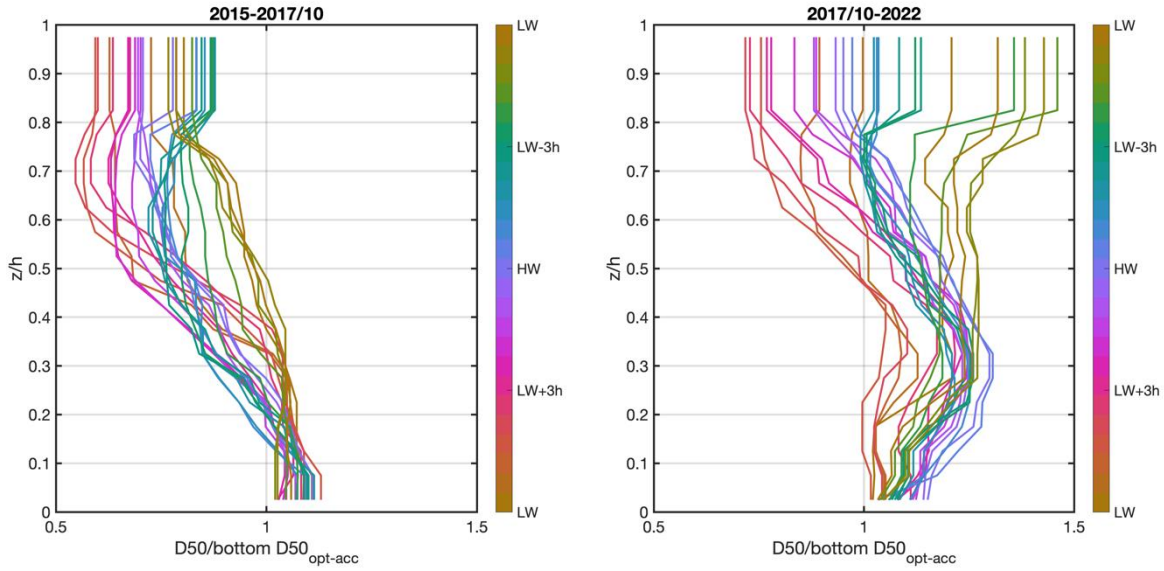

Figure 20: Optimal D50 extrapolation along the water column based on bottom $D50_{opt\text{-}acc}$ calculated from bottom SPMC for 2015-2017/10 (left) and 2017/10-2022 (right).

Declaration of interests

☒ The authors declare that they have no known competing financial interests or personal relationships that could have appeared to influence the work reported in this paper.

☐ The authors declare the following financial interests/personal relationships which may be considered as potential competing interests:

Highlights

Long term high frequency observations were analyzed to investigate the sediment dynamics at the interface between estuary and coastal sea

An original approach was developed to unify and inverse acoustic backscatter signal to SPM concentration

Instantaneous and residual sediment fluxes were computed and analyzed to apprehend sediment exchange dynamics between the estuary and the coastal sea in response to riverine and oceanic forcings.